An update to this article is included at the end

Journal of Theoretical Biology 365 (2015) 40–54

Contents lists available at ScienceDirect

Journal of Theoretical Biology

journal homepage: www.elsevier.com/locate/yjtbi

Characterizing spiking in noisy type II neurons

Katarína Bod'ová [a,*], David Paydarfar [b,c], Daniel B. Forger [d]

[a] Institute of Science and Technology Austria (IST Austria), Am Campus 1, Klosterneuburg A-3400, Austria
[b] Department of Neurology, University of Massachusetts Medical School, Worcester, MA, United States
[c] Wyss Institute for Biologically Inspired Engineering, Harvard University, Boston, MA, United States
[d] Department of Mathematics and Department for Computational Medicine and Bioinformatics, University of Michigan, Ann Arbor, MI, United States

HIGHLIGHTS

- The effect of channel stochasticity and input variability on a neuron is studied.
- A probabilistic switching model is proposed to capture the neuronal firing.
- The model explains firing rate statistics besides the mean firing rate.
- The model is easily applicable to experimental recordings.

ARTICLE INFO

Article history:
Received 15 July 2014
Received in revised form
26 September 2014
Accepted 30 September 2014
Available online 12 October 2014

Keywords:
Hodgkin–Huxley model
Markov process
Stochastic transitions
Excitable systems

ABSTRACT

Understanding the dynamics of noisy neurons remains an important challenge in neuroscience. Here, we describe a simple probabilistic model that accurately describes the firing behavior in a large class (type II) of neurons. To demonstrate the usefulness of this model, we show how it accurately predicts the interspike interval (ISI) distributions, bursting patterns and mean firing rates found by: (1) simulations of the classic Hodgkin–Huxley model with channel noise, (2) experimental data from squid giant axon with a noisy input current and (3) experimental data on noisy firing from a neuron within the suprachiasmatic nucleus (SCN). This simple model has 6 parameters, however, in some cases, two of these parameters are coupled and only 5 parameters account for much of the known behavior. From these parameters, many properties of spiking can be found through simple calculation. Thus, we show how the complex effects of noise can be understood through a simple and general probabilistic model.

© 2014 The Authors. Published by Elsevier Ltd. This is an open access article under the CC BY-NC-ND license (http://creativecommons.org/licenses/by-nc-nd/3.0/).

1. Introduction

The stochastic opening and closing of ion channels generates electrical activity in neurons. With just a few channels, as would occur in small neurons or those with low channel densities, stochasticity of a channels opening and closing could impact a neurons electrical activity causing the timing of action potential firing to appear random. Randomness in action potential firing could also be caused by the inherent stochasticity of neurotransmitter release, as well as random inputs received by a neuron. For these reasons, neuroscientists have realized that an understanding of neuronal coding requires an understanding of how both inherent stochasticity within neuronal systems and external input variability affect the electrical activity of neurons. Understanding the role of noise in neural coding is particularly important since noise in neurons can play beneficial, and even essential roles (Faisal et al., 2008).

Understanding behavior of neuronal networks in a noisy environment meets many challenges. The computational techniques using channel-based neuronal models shed light into the dynamical features of neuronal networks but a major obstacle is the considerable computational power necessary for simulating networks of relevant sizes when resolving detailed voltage traces of all neurons. An accurate statistical description of action potential timing that avoids the complex simulation of the voltage traces could facilitate computational modeling of network's behavior. The present study focuses on a single neuron and proposes a statistical description of a spike timing that is simple enough to reduce the complexity of the simulation but on the other hand accurately reproduces important features of spike timing beyond the average firing rate.

With a great level of simplification a neuron may be thought represented by a probabilistic device processing noisy signals by its own inherently noisy encoding where the neuronal output is represented by a sequence of action potential times. Here we aim

* Corresponding author. Tel.: +43 2243 9000 3007.
E-mail addresses: kbodova@ist.ac.at (K. Bod'ová), david.paydarfar@umassmed.edu (D. Paydarfar), forger@umich.edu (D.B. Forger).

http://dx.doi.org/10.1016/j.jtbi.2014.09.041
0022-5193/© 2014 The Authors. Published by Elsevier Ltd. This is an open access article under the CC BY-NC-ND license (http://creativecommons.org/licenses/by-nc-nd/3.0/).

to characterize how noise in neurons affects the timing of these action potentials. If a neuron receives constant or random (time homogeneous) inputs the simplest prediction, based solely on the average firing rate, would imply a Poisson process for the action potential generation with exponentially distributed times between spikes. However, the experimental data we have at hand suggest deviations from the Poisson process and implies a need for a more advanced probabilistic framework. Our goal is to construct a structurally more complicated probabilistic model that gives a mechanistic explanation on the processes present and to test it in various experimental and numerical settings.

Previous experimental work applied random currents to the cell and recorded the spiking patterns that resulted (Paydarfar et al., 2006; Tateno et al., 2004) or recorded variability in neuronal membrane potential (Verveen and Derksen, 1968). The experiments in Paydarfar et al. (2006), renalyzed in the present study to evaluate our modeling framework, were performed in the squid giant axon that has very high channel densities. Because of that, the effect on membrane potential of channel stochasticity in this neuron is negligible compared to input current variability. On the other hand, since designing an experimental procedure that would allow adjusting the channel densities is difficult (it would require selectively disabling some proportion of the channels), we use numerical simulations for a wide range of channel densities to study the effects of variability originating from a channel noise in the absence of the applied current noise.

We study this in type II neurons, showing two electrical states, one of quiescence, and one of repetitive firing of action potentials with relatively invariant spike frequency with respect to input current level. This broad class includes many neurons and models, including the original Hodgkin–Huxley model (Hodgkin, 1948; Hodgkin and Huxley, 1952). The sharp transition to oscillations in type II neurons associated with a destabilization of the quiescent state can be described mathematically by a subcritical Hopf bifurcation as opposed to type I neurons where a saddle-node bifurcation on an invariant circle captures a gradual response of the firing rate on the injected current. However, variability in either the input current or in the channel dynamics changes this rapid response to gradual even for the II neurons that are considered here and thus makes the type II neuron behave in a similar way to the type I neuron. Since the timing of an individual spike is stochastic, we seek to explain the average rate of action potential firing as well as the distribution of times between spikes. An additional goal in our simulation approach is to study effects of sodium channel versus potassium channel variability that have been previously shown to play a role both for single Hodgkin–Huxley type neurons (Chow and White, 1996) and for networks of neurons of Hodgkin–Huxley type (Ozer et al., 2009).

In order to simulate noisy channel dynamics in neurons, two distinct techniques have been developed. One technique uses a Kinetic Monte Carlo (KMC) approach, also called the Gillespie scheme (Gillespie, 1977) to simulate the stochasticity of the opening and closing of individual channels (Clay and DeFelice, 1983; Chow and White, 1996; Schneidman et al., 1998; White et al., 2000; Skaugen and Walløe, 1979; Rowat, 2007). Another technique takes a Langevin stochastic (LS) approach where noise is included in the model's ordinary differential equations that are then simulated using standard techniques (see Goldwyn and Shea-Brown, 2011; Fox, 1997; Ozer and Ekmekci, 2005; Schmid et al., 2006; Bazsó et al., 2003 for multiplicative noise and Bazsó et al., 2003; Saarinen et al., 2006 for constant-amplitude noise techniques). Here we use both methods (where the particular implementation of the KMC method uses an independent subunit approach (Goldwyn and Shea-Brown, 2011) and the LS method uses the Fox method Fox, 1997; Fox and Lu, 1994) to acquire a dataset for electrical activity of neurons with channel noise, complementary to the experimental data of noisy inputs.

We find that both experimental and simulation approaches give a coherent picture of noisy neuronal spiking. We use three case studies: (a) a computational study with channel noise; (b) an experimental study with input current noise; and (c) an experimental data reflecting both sources of noise. These approaches show complementary faces of the noisy neuronal behavior, with either channel noise or input current noise or both noise sources being in play. We aim to compare and contrast the similarities and differences between effects of experimental variable inputs and numerical noisy channels and to provide a characterization of the neuronal behavior on a level that is independent of where the randomness originates from. We show how the seemingly complex distribution of interspike intervals under various sources of randomness can be reproduced with a simple and intuitive mathematical model (SQ model) with just a few parameters capturing various noise properties. This model can be used to explain both numerically simulated and experimentally observed spike trains and in particular the effects of stochasticity on the average firing rate, distribution of interspike intervals and the distribution of burst lengths. This work provides a framework for understanding the behavior of noisy neurons whose dynamics are similar to the Hodgkin–Huxley equations. The SQ model provides an extensive reduction in computer simulation complexity in comparison with the approaches using complete voltage trace simulations.

2. Methods and models

2.1. The probabilistic SQ model

Several theoretical approaches have been used to study noise-induced activation in bistable systems. Probabilistic models have been designed to study multi-state problems with a random switching between states (Longtin et al., 1991; Rowat, 2007; Rowat and Greenwood, 2011). We use this approach to capture the nonlinear dynamics of the Hodgkin–Huxley model. Fig. 1, panels (B) and (C) show density of trajectories in the HH model around the steady state with channel noise simulated using the LS approach in the bistable regime. The Hodgkin–Huxley model has four variables, however, we plot only two of the variables at a time. The density is plotted in a close neighborhood of the fixed point, similarly as in works (Rowat, 2007; Rowat and Greenwood, 2011; Paydarfar and Buerkel, 1997) to demonstrate the sensitivity to noise. Trajectories spend most of the time around the fixed point and nearby the limit cycle (obtained numerically by starting at a random initial condition and discarding the transient dynamics). However, as opposed to the deterministic case, they often cross between the fixed point and the limit cycle attraction regions. This switch between the limit cycle behavior and looping around the fixed point, typically referred to as subthreshold oscillations, occurs in a small part of the domain where the fixed point is closest to the limit cycle.

Based on the behavior of the system, we consider two states, similar to what was suggested in Rowat and Greenwood (2011), Longtin et al. (1991) - the repetitively firing state (S) and the quiescent state (Q) where the trajectory fluctuates around a steady state as the locally linear dynamics of the system predicts in the proximity of the fixed point. We assume that when the model is in the repetitively firing state the time between spikes with no intervening subthreshold oscillations is normally distributed and that also the noise induced subthreshold oscillations have a period drawn from a normal distribution with parameters

- S $\sim\mathcal{N}(\mu_1,\sigma_1)$ – the spiking state,
- Q $\sim\mathcal{N}(\mu_2,\sigma_2)$ – the quiescent state.

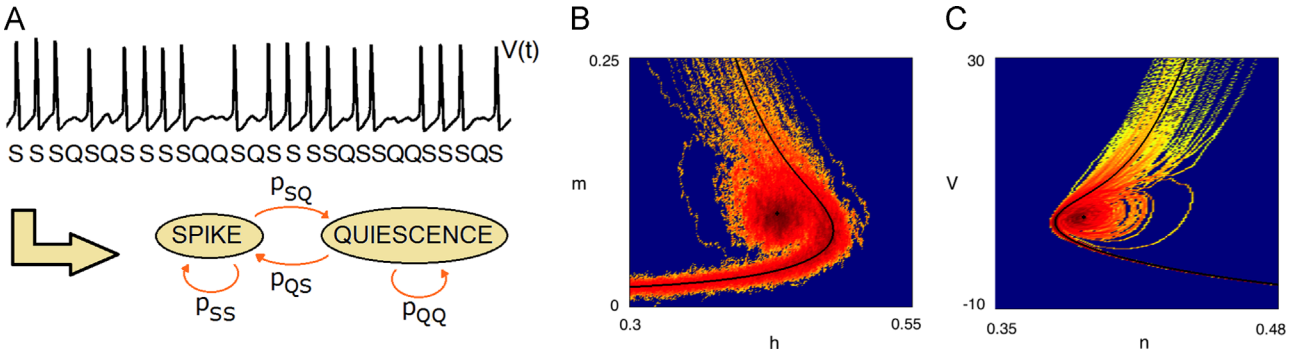

Fig. 1. The probabilistic SQ model. (A) The firing sequence is split into a sequence of states S and Q (see Section 2.4), where S corresponds to a spike and Q corresponds to a quiescent state. Based on the number of S→Q and Q→S transitions the transition probabilities p_{SQ}, p_{QS} and p_{SS}, p_{QQ} between the states may be estimated. The duration of each state is a random variable with a constant mean and variance. (B-C) The density of the trajectory around the steady state for $I=8$ μA/cm^2 using the Langevin method calculated by binning a long stochastic simulation with fixed time step into small square bins – 2D histogram. The steady state of the Hodgkin–Huxley model (that changes with applied current) lies in a close proximity of the limit cycle, as indicated by the black dot (steady state) and black curve (limit cycle). Trajectories of the stochastic model either fire action potentials, i.e., follow the limit cycle, or stay in the quiescent regime, i.e., in the neighborhood of the rest state where they also fluctuate around the steady state in the same fashion as action potentials but with a significantly smaller amplitude. Randomness causes switching from one pattern to the other. Density of trajectories varies from bright yellow (small density) to dark red (high density) where blue corresponds to zero density. (For interpretation of the references to color in this figure caption, the reader is referred to the web version of this article.)

where

- μ_1, σ_1 – mean and standard deviation of the action potential duration,
- μ_2, σ_2 – mean and standard deviation of the subthreshold oscillation duration.

Since the subthreshold oscillations can be thought of as trajectories in the state space fluctuating around the steady state with a smaller amplitude than action potentials it is reasonable to expect that $\mu_2 < \mu_1$ (typical situation). The presence of these fluctuations is evident in the ISI histograms presented later in the text, in particular for small noise where a clear separation of modes suggests that the action potentials are separated by an integer number of Q events. The estimated values of μ_2 as well as other parameters of the SQ models are summarized in Table 1.

The SQ model, described by the scheme in Fig. 1(A), characterizes transitions between the states S and Q that are Markovian, i.e., history independent. The switching probabilities depend on the magnitude and source of noise as well as on the value of input current and are defined by

- p_{SQ} – probability that the current spiking state is followed by a quiescent state,
- p_{QS} – probability that the current quiescent state is followed by a spiking state,
- p_{QQ} – probability of staying in the quiescent state after starting in this state,
- p_{SS} – probability of staying in the spiking state after starting in the spiking state.

where by definition $p_{QQ}+p_{QS}=1$ and $p_{SQ}+p_{SS}=1$. The Markovian property may be validated using numerical simulations of the HH model by showing that after one period in either state, the system returns to the noise sensitive region where it can transition from one state to another (as in Fig. 1(B-C)) and forget its previous evolution (more detailed analysis for the Morris–Lecar model can be found in Rowat and Greenwood (2011)). Perhaps surprisingly, the stochastic Hodgkin–Huxley model shows similar switching behavior even outside of the bistability region (characterized by moderate values of applied current). The reason for this is that bistable behavior in the stochastically perturbed Hodgkin–Huxley model is accompanied by a smooth increase of the firing rate for increasing applied current (Clay and DeFelice, 1983; Chow and White, 1996; White et al., 2000; Schmid and Hanggi, 2007) unlike in the deterministic case when the transition is rapid and emerges via a subcritical Hopf bifurcation.

Table 1
The parameter values of the SQ model estimated to fit the computed histograms (LS method) and experimental histograms from Paydarfar et al. (2006) and Kononenko and Dudek (2004). Note that both the numerical and experimental histograms for the squid giant axon are normalized so that the unit duration corresponds to the stochastically unforced period T (that is approximately 11.8, 11.2, 12.4, 11.7 ms for cases $I_{rms}=0.13, 0.20, 0.35, 0.43$ μA/cm^2 and 16.6 ms for the LS method where $I=8$ μA/cm^2).

Data source/Parameter	p_{SQ}	p_{QS}	μ_1	μ_2	σ_1	σ_2
Numerical data:						
$N=10^6$	0.09	0.26	0.9398	0.7682	0.0452	0.0602
$N=10^4$	0.17	0.44	0.9337	0.7229	0.0542	0.1205
N=2500	0.20	0.66	0.9036	0.6627	0.0994	0.1928
N=625	0.21	0.81	0.8735	0.2410	0.0813	0.1205
Experiments, squid:						
$I_{rms}=0.13$ μA/cm^2	0.0029	1.00	1.0093	1.0082	0.0489	0.1090
$I_{rms}=0.20$ μA/cm^2	0.07	0.13	1.0023	0.2462	0.0640	0.0832
$I_{rms}=0.35$ μA/cm^2	0.15	0.46	0.9780	0.4938	0.0850	0.1103
$I_{rms}=0.43$ μA/cm^2	0.15	0.74	0.9810	0.9030	0.0959	0.1346
Experiments, SCN:						
Fig. 3 (C, red)	0.94	0.58	82.47	82.47	12.64	57.77
Fig. 3 (C, blue)	1.00	0.63	82.47	164.93	12.64	93.01
Fig. 3 (D, red)	1.00	0.56	76.12	79.93	5.67	55.07
Fig. 3 (D, blue)	1.00	0.66	76.12	175.08	5.67	97.30

The SQ model allows for a characterization of the statistical properties of the spike train based on basic properties of this stochastic process. We use the ISI distribution and the burst size distribution to represent the process, however, different choices can be made allowing for an suitable description of particular features we wish to capture.

2.2. Interspike interval distribution

The explicit dependence of the mean firing rate on transition rates p_{SQ} and p_{QS} and on mean durations of the firing and quiescent state μ_1 and μ_2 can be directly calculated for the simple probabilistic SQ model in a connection with the ISI distribution.

Since the stochastic SQ process is memoryless, we may decompose the inter-spike interval consisting of a sequence of firing (S) and quiescence (Q) into distinct independent firing events SS, SQS, SQQS, etc. with probabilities

$$P[\mathrm{SS}] = p_{\mathrm{SS}},$$
$$P[\mathrm{SQS}] = p_{\mathrm{SQ}}p_{\mathrm{QS}},$$
$$P[\mathrm{SQQS}] = p_{\mathrm{SQ}}p_{\mathrm{QQ}}p_{\mathrm{QS}},$$
$$P[\mathrm{SQQQS}] = p_{\mathrm{SQ}}p_{\mathrm{QQ}}^2p_{\mathrm{QS}}, \cdots$$

Under assumptions of the SQ model the ISI distribution, i.e. the distribution of the time between two consecutive spikes, defined by a probability function

$$P_{\mathrm{ISI}}(t) := P[\text{time between two consecutive spikes} = t], \tag{1}$$

has an exponential tail, i.e. $P_{\mathrm{ISI}}(t) \sim Ae^{-Bt}$ for large t. This property of the SQ model, consistent with the findings of Chow and White (1996), follows from an observation that the peak heights of $P_{\mathrm{ISI}}(t)$ decay geometrically by a factor p_{QQ} except for the first peak that decays by a different factor $p_{\mathrm{SQ}}p_{\mathrm{QS}}/p_{\mathrm{SS}}$.

We can calculate the rate of this decay using the fact that $P_{\mathrm{ISI}}(t+\mu_2) = p_{\mathrm{QQ}}P_{\mathrm{ISI}}(t)$ and derive an estimation formula for the probability p_{QQ} given the constants μ_2 and B:

$$p_{\mathrm{QQ}} = e^{-B\mu_2}. \tag{2}$$

and represent the ISI distribution as a mixture of uncorrelated Gaussian distributions with a density:

$$\begin{aligned} f(x,\mu_1,\mu_2,\sigma_1,\sigma_2,p_{\mathrm{SQ}},p_{\mathrm{QS}}) &= p_{\mathrm{SS}}\cdot g(x,\mu_1,\sigma_1^2) + p_{\mathrm{SQ}}p_{\mathrm{QS}}\cdot g(x,\mu_1+\mu_2,\sigma_1^2+\sigma_2^2) \\ &\quad + p_{\mathrm{SQ}}p_{\mathrm{QQ}}p_{\mathrm{QS}}\cdot g(x,\mu_1+2\mu_2,\sigma_1^2+2\sigma_2^2) \\ &\quad + p_{\mathrm{SQ}}p_{\mathrm{QQ}}^2p_{\mathrm{QS}}\cdot g(x,\mu_1+3\mu_2,\sigma_1^2+3\sigma_2^2)+\cdots \end{aligned}$$

where $g(x,\mu,\sigma^2)$ is a probability density of a Gaussian distribution with mean $\mu$and variance σ^2.

Then the mean inter-spike interval can be calculated as

$$\begin{aligned} \mathbb{E}[\mathrm{ISI}] &= \mu_1 p_{\mathrm{SS}} + (\mu_1+\mu_2)p_{\mathrm{SQ}}p_{\mathrm{QS}} + (\mu_1+2\mu_2)p_{\mathrm{SQ}}p_{\mathrm{QQ}}p_{\mathrm{QS}} \\ &\quad + (\mu_1+3\mu_2)p_{\mathrm{SQ}}p_{\mathrm{QQ}}^2p_{\mathrm{QS}} + \cdots = \mu_1 + \mu_2\frac{p_{\mathrm{SQ}}}{p_{\mathrm{QS}}} > \mu_1. \end{aligned} \tag{3}$$

The last equality follows from properties of generalized geometric sequences. The relationship implies that the average firing rate $1/\mathbb{E}[\mathrm{ISI}]$ in the superthreshold regime should be smaller than the firing rate in the absence of noise μ_1. In contrast, the firing rate in the subthreshold noisy regime is always larger compared to noise-free regime where no spikes are seen. If the noise level is too strong the SQ model, and in particular the decrease in the firing rate due to noise, is no longer valid due to the fact that the excursion around the limit cycle could be greatly affected and sped up by large noise as observed in Tateno et al. (2004) implying a smaller value of μ_1. On the other hand, a natural assumption of the increase of p_{QS} and the decrease of p_{SQ} with increasing the input current yields that the firing rate also increases, which is in agreement with our numerical results and known results in the literature (White et al., 2000; Schmid and Hanggi, 2007).

Similar calculation to (3) for the second moment yields

$$\begin{aligned} \mathrm{Var}[\mathrm{ISI}] &= \sigma_1^2 p_{\mathrm{SS}} + (\sigma_1^2+\sigma_2^2)p_{\mathrm{SQ}}p_{\mathrm{QS}} + (\sigma_1^2+2\sigma_2^2)p_{\mathrm{SQ}}p_{\mathrm{QQ}}p_{\mathrm{QS}} \\ &\quad + (\sigma_1^2+3\sigma_2^2)p_{\mathrm{SQ}}p_{\mathrm{QQ}}^2p_{\mathrm{QS}} + \cdots = \sigma_1^2 + \sigma_2^2\frac{p_{\mathrm{SQ}}}{p_{\mathrm{QS}}} > \sigma_1^2. \end{aligned} \tag{4}$$

Expressions (3) and (4) allow us to calculate a noise-to-signal ratio that is often used in the context of coherence resonance when analyzing the regularity of spikes in Hodgkin–Huxley model (Gong et al., 2009; Lee and Kim, 1999) or other more general models (Pikovsky and Kurths, 1997) defined as $R = \sqrt{\mathrm{Var}[\mathrm{ISI}]}/\mathbb{E}[\mathrm{ISI}]$.

2.3. Burst size distribution

The SQ model can be also used to understand the burst size distribution, representing number of subsequent spikes in a spike train, defined by a probability function

$$P_B(n) := P[\text{number of S states between two subsequent Q states} = n]. \tag{5}$$

Each burst may be represented by an event that has a corresponding probability

$$P[QSQ] = p_{\mathrm{QS}}p_{\mathrm{SQ}},$$
$$P[QSSQ] = p_{\mathrm{QS}}p_{\mathrm{SS}}p_{\mathrm{SQ}},$$
$$P[QSSSQ] = p_{\mathrm{QS}}p_{\mathrm{SS}}^2p_{\mathrm{SQ}}, \cdots$$

The burst size distribution then has an exponential form $P_B(t) \sim ae^{-bt}$ that is valid for any t unlike in the case of the ISI where the first mode of the distribution did not follow the exponential law. Using the fact that $P_B(n+1) = p_{\mathrm{SS}}P_B(n)$ the transition probability p_{SS} may be approximated as

$$p_{\mathrm{SS}} = e^{-b}. \tag{6}$$

This provides a tool for an estimation of transition probability p_{SS} from the experimental data. The burst size distribution may be also represented by a mixture of individual burst events of integer lengths implying

$$\mathbb{E}[\mathrm{B}] = p_{\mathrm{QS}}p_{\mathrm{SQ}} + 2p_{\mathrm{QS}}p_{\mathrm{SS}}p_{\mathrm{SQ}} + 3p_{\mathrm{QS}}p_{\mathrm{SS}}^2p_{\mathrm{SQ}} + \cdots = \frac{p_{\mathrm{QS}}}{p_{\mathrm{SQ}}}. \tag{7}$$

The estimation formulas (2) and (6) for p_{QQ} and p_{SS} require a prior knowledge of exponential decay rates B and b as well as the average subthreshold oscillation time μ_2. Constants B and b are obtained from the experimental data for the squid giant axon using least squares minimization to an exponential function (performed on a logarithmic scale).

2.4. Estimation of model parameters

The SQ model is characterized by six parameters that need to be robustly estimated from the available firing rate data. Even thought the character of the data may differ between various experiments, the estimation of the SQ model's parameters allows for their flexibility and an appropriate estimation strategy may thus be tailored to the needs of a particular problem.

The most straightforward but also very naive procedure for obtaining transition rates p_{QS} and p_{SQ} is to decompose the electrical activity of the neuron to states S and Q (the method will be outlined below). Once the temporal data are converted into the sequence of discrete events S and Q, the number N_X of transitions X={SS, SQ, QS, QQ} is extracted and the transition probabilities are estimated as

$$p_{\mathrm{SS}} = 1 - p_{\mathrm{SQ}} = \frac{N_{\mathrm{SS}}}{N_{\mathrm{SS}}+N_{\mathrm{SQ}}}, \quad p_{\mathrm{QQ}} = 1 - p_{\mathrm{QS}} = \frac{N_{\mathrm{QQ}}}{N_{\mathrm{QQ}}+N_{\mathrm{QS}}}. \tag{8}$$

The decomposition of the electrical signal to the S and Q states may be difficult if the duration of the states is highly variable. This is typical for neurons with large noise, i.e., low channel densities. While the S states can be found by thresholding the voltage trace, accurate detection of Q states (connected to accurate estimate of μ_2) is more subtle. Our approach is based on a knowledge of μ_1 and μ_2:

- *Identification of the states*: Obtain the average time μ_1^* and μ_2^* of S and Q state using position of the first two peaks of the ISI distribution. Use a high enough threshold to identify the times of spikes and compute successive times between spikes Δt. Estimate the number of Q states between the consecutive

spikes as

$$n_Q = \left\lfloor \frac{\Delta t - \mu_1^*}{\mu_2^*} \right\rfloor \quad (9)$$

where the brackets $\lfloor \cdot \rfloor$ stand for the floor function – the largest previous integer. Reconstruct the sequence of S and Q states according to the obtained counts n_Q and compute number of transitions between states that enter into (8).

To avoid difficulties with identification of S and Q states in the spike train we use two approaches based on a statistical description of the firing behavior to estimate the ISI distribution:

- *Least square minimization*: Minimize the error $S(\mu_1, \mu_2, \sigma_1, \sigma_2, p_{SQ}, p_{QS})$ between the ISI distribution and the mixture distribution where

$$S(\mu_1, \mu_2, \sigma_1, \sigma_2, p_{SQ}, p_{QS}) = \sum_i [f(x_i, \mu_1, \mu_2, \sigma_1, \sigma_2, p_{SQ}, p_{QS}) - \mathrm{ISI}(x_i)]^2 \quad (10)$$

  where x_i correspond to positions of ISI histogram bins. In particular, if the ISI distribution is multimodal, obtain the average time μ_1^* and μ_2^* of S and Q state using position of the first two peaks of the ISI distribution and minimize $S(\mu_1^*, \mu_2^*, \sigma_1, \sigma_2, p_{SQ}, p_{QS})$ to find the remaining parameters. On the other hand, if the distribution has a single peak use only μ_1^* (location of the ISI distribution peak) and proceed with minimization of $S(\mu_1^*, \mu_2, \sigma_1, \sigma_2, p_{SQ}, p_{QS})$.
- *Matching statistical properties*: Use statistical information about the rates of decay and the statistics of the ISI distribution and the burst size distribution of the spike train to estimate the transition probabilities using the following constraints:
  - Estimate parameter μ_1 by μ_1^* as above.
  - Estimate μ_2 by μ_2^* if the distribution is multimodal.
  - Use constraints (2)–(6).

  One can use a subset of these constraints in combination with least squares optimization or for simplicity take $\mu_1 = \mu_2$ or $\sigma_1 = \sigma_2$.

The SQ model gives flexibility in terms of a parameter fitting method and it does not rely on a classification of the S and Q states that may be difficult to obtain from measurements of electrical activity of neurons.

3. Results

Based on our geometric arguments for the HH model (Fig. 1(B)), we consider a probabilistic two-state SQ model introduced in the Methods section. We assume that the system is either in the repetitively firing state (S) or in the quiescent state (Q) with a random normally distributed period for each. Unlike the deterministic systems, where S only occurs above a threshold applied current, we note that spiking can occur in the stochastic model even when the applied current is zero and becomes more likely at higher input currents. Thus, we allow both states in our mathematical description regardless of the applied current. The transition probabilities p_{QS} and p_{SQ} between the states in

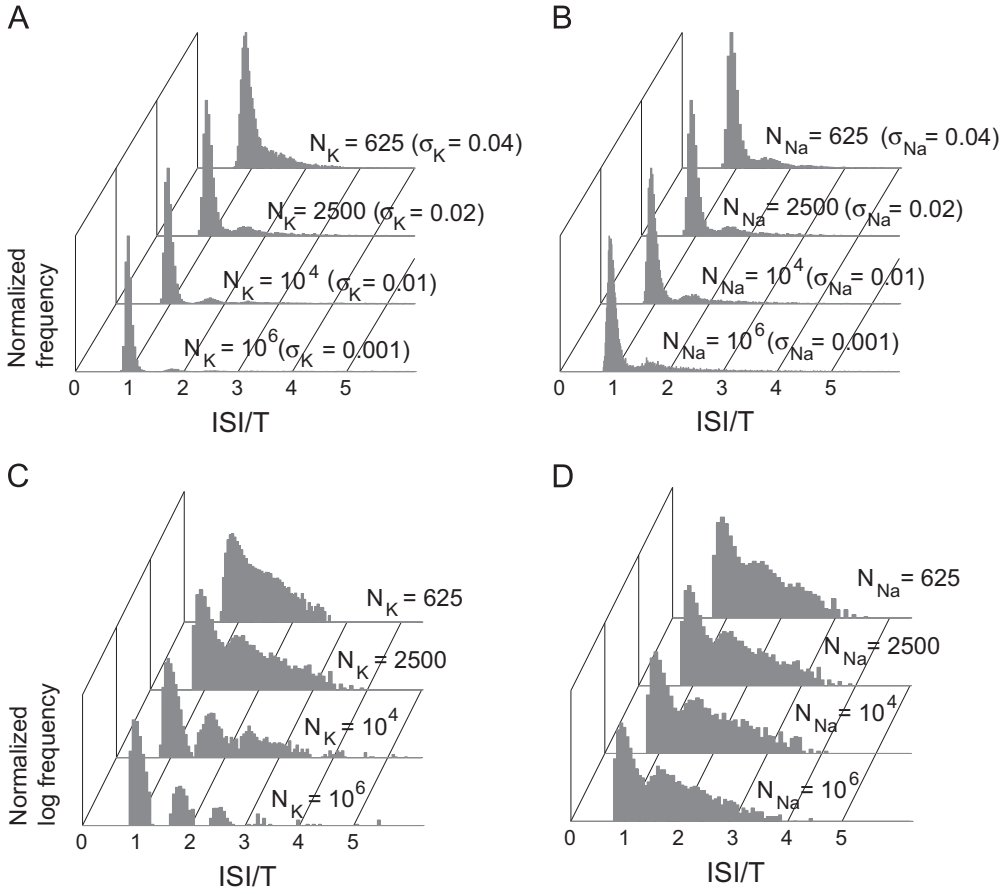

Fig. 2. (A)–(B) Multimodality and effects of sodium and potassium channel noise on the normalized ISI distribution for the Fox method, also showed on a logscale on (C)–(D). The ISI histograms are found numerically for $I = 8\ \mu A/cm^2$. The histogram changes from multi-peaked to exponentially decaying as randomness increases. This is more visible when changing potassium noise as opposed to sodium noise where the same difference in channel number results in a smaller difference in the distribution shape. ISI/T is plotted on the horizontal axis while $T = 16.6$ ms is the period in the stochastically unforced system.

Fig. 1(A) depend on the applied current as well as on the source and magnitude of randomness in the neuron.

3.1. Multimodality and distribution tails

Fig. 2 is obtained by numerical simulations of the Fox method with the input current 8 $\mu A/cm^2$ so that the quiescent state and repetitive firing state are both stable in the absence of noise (one should note that in the case of low and high input currents, without bistability of the rest state and the limit cycle, the results would be similar), see Appendix A for details on the Fox method. Fig. 2 gives a justification of the fact that subthreshold oscillations have a well-defined duration that is random with a single-peaked and rather narrow distribution. Particularly for small potassium variabilities the distribution consists of multiple narrow peaks of decreasing height where the first peak represents the time-distribution of the action potential, the second peak corresponds to the time of AP plus one subthreshold oscillation, etc. Thus the mean length as well as the variance of the subthreshold oscillations can be defined by subtracting the center of the second peak of the distribution from the center of the first one when obtaining mean and substracting the corresponding variances for the second moment. Because there is a clear gap between the peaks and the peaks are roughly bell-shaped and symmetric (similarly to the ISI histograms in SCN neurons in Kononenko and Dudek, 2004) we postulate that the normal distribution gives a solid estimate of both the distribution of ISI durations and the distribution of the subthreshold oscillations. Note that for higher levels of potassium noise these distributions need to have larger variances to obtain a smeared shape of the distribution.

For low levels of potassium noise, a multimodal distribution was found with peaks centered approximately around the integer multiples of the stochastically unforced period T (ISI/T plotted on the horizontal axis). Positions of these modes depend on μ_1 and μ_2 ($\mu_1 \approx \mu_2$). The peak of these modes decreased exponentially as the ISI increased. However, the first (and largest) peak did not fit this exponential decay, see Fig. 2(C and D). This property is preserved in the SQ model where the first peak carries a mass of p_{SS}, second one carries $p_{SQ}p_{QS}$ and the remaining peaks decay by a constant factor p_{QQ} and is consistent with experimental studies for instance in the study of sporadic apnea (Paydarfar and Buerkel, 1997). For high levels of potassium noise, the distribution changed from multimodal to single peaked and showed an exponential tail, consistent with the simulations of Rowat and Greenwood (2011) for the Morris–Lecar model. In all cases, there was a refractory period, in that ISI values were never below 8 ms. It is worth noting that the simplest probabilistic spiking model, i.e. Poisson process for the spike times (carries information about average firing rate only), implies exponential distribution of the ISI distribution, unlike the experimental and numerical data where just the tail of the distribution has an exponential decay.

3.2. SQ model performance and universality to noise source

To test the ability of the SQ model to capture statistical properties of the spike trains we use three distinct case studies:

(a) A computational study with channel noise using a continuous description (model description and numerical methods are presented in Appendix A).

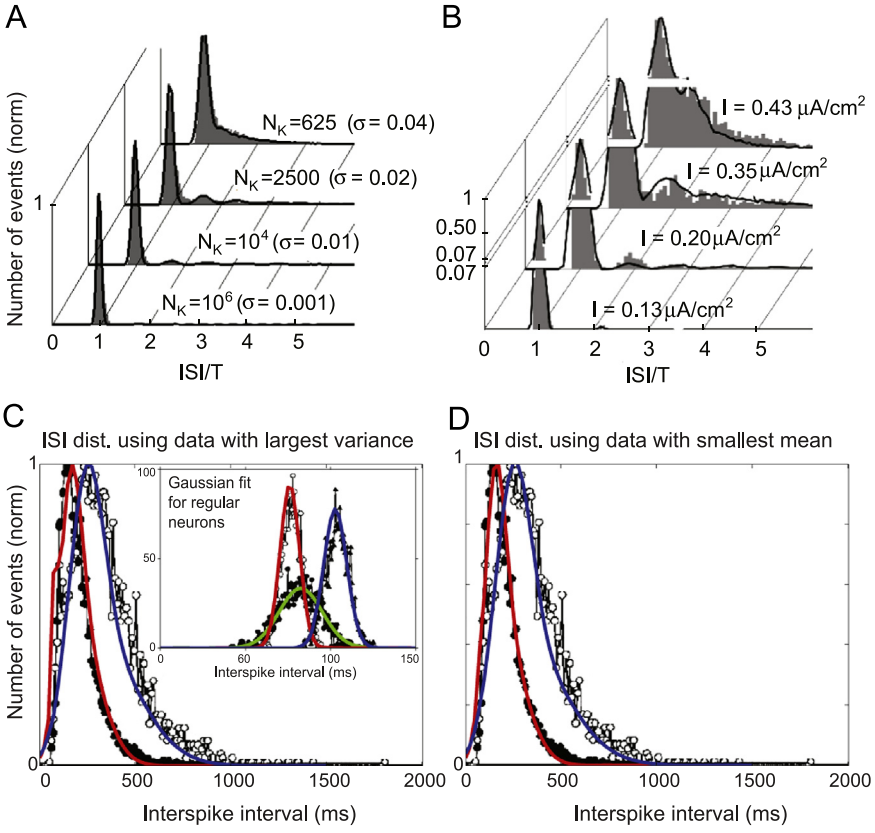

Fig. 3. Fitting the SQ model to numerical and experimental data. (A) Simulation of the ISI distribution by the LS method (gray histograms) versus the SQ model (black lines) for sodium channel number $N_{Na} = 2500$ and $I=8$. (B) Experimental recordings of the squid giant axon from Paydarfar et al. (2006) (gray histograms) with the SQ model distribution (black lines). These plots show the accuracy of the SQ model in representing the simulations and experimental data. All data were normalized with respect to the deterministic oscillations period T (that has been measured experimentally as approximately 11.8, 11.2, 12.4, 11.7 for cases $I=0.13$, $I=0.20$, $I=0.35$, $I=0.43$ $\mu A/cm^2$) therefore the first peak is centered around one. (C), (D) Fitted ISI histograms from Kononenko and Dudek (2004) that correspond to regular firing neurons in the upper right corner of (C) are fitted to a Gaussian distribution with mean μ_1 and variance σ_1. These are used in the SQ model to fit the ISI distribution of the irregularly spiking neurons on (C) and (D). Experimental readings are in black, our fits in red/blue/green. (For interpretation of the references to color in this figure caption, the reader is referred to the web version of this article.)

(b) An experimental study with input current noise (data from Paydarfar et al., 2006 and formerly unpublished data for identical level of input current variability), see Appendix B for further details.
(c) Experimental data reflecting both channel noise and input noise (Kononenko and Dudek, 2004).

(a) For each ISI distribution calculated in our numerical simulations, presented in Fig. 2, we fit the SQ model to determine which features of the ISI distribution it can accurately reproduce. We find that it is very accurate in reproducing the numerically computed ISI distributions obtained using LS method, including both the multimodal and the single peak-exponential tail distributions in Fig. 3(A) in all parametric noise regimes. The inferred SQ model parameters (μ_1, μ_2, σ_1, σ_2, p_{SQ}, p_{QS}) summarized in Table 1 were obtained by least square minimization method described in Methods. The SQ model is very robust to small changes in its parameters and a very good match of the data can be obtained for a large set of parameters. We have also checked whether the transition probabilities are consistent with the data by splitting the spike train to a sequence of S, Q states based on our knowledge of μ_1 and μ_2 with the method outlined in Section 2.4. The transition probabilities estimated from (8) were consistent with the ones fitted to the ISI histograms.

(b) To further check the SQ model, we sought to determine whether the SQ model could represent formerly published experimental data collected from squid giant axons with a noisy input current (Paydarfar et al., 2006) given in terms of ISI histograms and burst size distribution. The SQ model (with least squares minimization used to infer parameters) accurately represented this experimental data as well (Fig. 3(B)), however, for a distinct set of parameters (Table 1). This shows that the relatively simple SQ model gives enough variability to provide an accurate description of the statistical behavior of noisy type II neurons and their mathematical models. In addition, it is applicable to the behavior arising from noisy input currents as well as stochastic channel dynamics and the properties of noise reflect in the values of the SQ parameters.

Fig. 4(A) shows new experimental data for ISI distribution and burst size distribution, described in detail in Appendix B. During the length of the experiment there was a total of 1404 spikes. The data shows the longest burst to have 76 spikes in a row and the most probable burst sizes present in the data had either one spike or four consecutive spikes, each one observed 15 times. To visualize the burst size distribution the data was binned into 20 equally wide bins – some of them unpopulated. The well populated part of the figure (up to 50 spikes per burst) was fitted to an exponential using a logarithmic scale to obtain an estimate for b. Also, the tail of the ISI distribution in Fig. 4(B) was fitted to exponential to obtain B and μ_2 was set equal to μ_1 – the time for which the ISI histogram reaches the maximal value. Therefore the parameters μ_1, μ_2 and transition rates in the SQ model were inferred using (2) and (6). Parameters σ_1 and σ_2 were fitted using least squares minimization to match the width of the ISI distribution peak properties. The SQ model was then simulated and compared with the distributions, showing an excellent match with the burst size distribution and a good match with the ISI distribution.

(c) Fig. 3(C) and (D) features the SQ model approximation of the regularly and irregularly firing SCN neurons from Kononenko and Dudek (2004). A universal SQ model is fitted to capture both types of neurons by a single model with a single parameter set to suggest that a universal mechanism is compatible with both observed types of behavior. The parameters of the model were obtained first by fitting a Gaussian to the regularly spiking neurons (obtaining μ_1 and σ_1) and then using (3), (4) and (2) to infer the transition probabilities and σ_2 by matching the statistical properties of the irregularly spiking data (we chose $\mu_2 = \mu_1$ when leading to $p_{SQ} \leq 1$, otherwise we inferred μ_2 such that $p_{SQ} = 1$). The SQ model shows a solid agreement with the experimental data on Fig. 3.

One of the main reasons to consider an SQ model is its computational efficiency in comparison with simulating the full voltage traces. This property is extremely important if one wants to simulate large coupled neuronal networks. The coupling, however, brings additional SQ model parameter dependence on the activity of the remaining neurons that needs to be investigated further. Therefore it is essential that the SQ model can truthfully capture the properties of a single neuron firing for a broad class of neurons. It is interesting to note that the patterns of ISI distributions, developed through simulations of channel noise, closely resemble those found experimentally in the squid giant axon for noisy input currents (Paydarfar et al., 2006) but match also the SCN data of Kononenko and Dudek (2004). The three case studies demonstrate an applicability of the SQ model to different neurons where different sources of noise prevail and that it can capture the statistical distributions (ISI histogram, burst size distribution) with a great accuracy.

3.3. Sensitivity to sodium and potassium variability

Two types of distributions (multimodal and single peaked) were observed for different levels of potassium and sodium noise in Fig. 2(A–D). We observe that, in response to changes in the

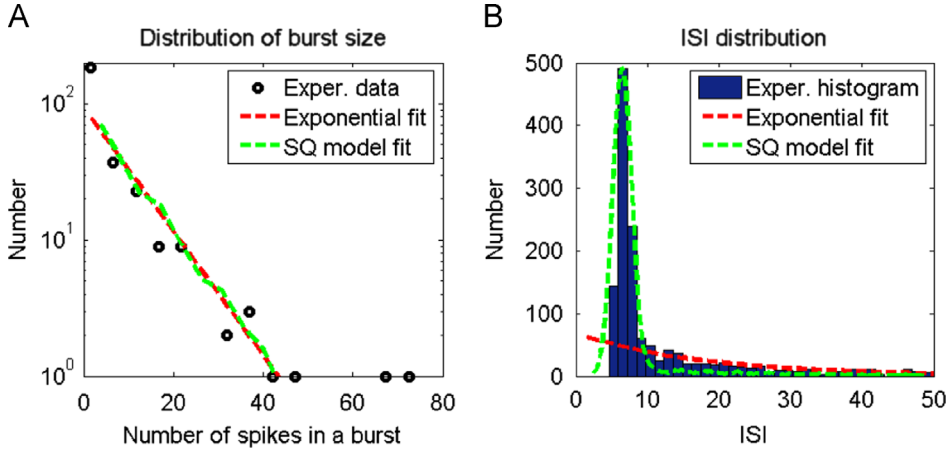

Fig. 4. Experimental results for the firing activity of the squid giant axon fitted to the SQ model. (A) Burst size distribution and (B) inter-spike interval distribution.

sodium noise, the ISI distribution shows only weak dependence of the distribution shape compared to potassium variability that affects the multimodality stronger. This is particularly well visible in Fig. 2 on the logplots of ISI distribution. Evidence for the large impact of potassium currents can be found in Stiefel et al. (2012) for irregularly spiking cortical interneurons but also in the computational neuronal network study (Ozer et al., 2009) where the topology of the network that produces maximal firing rate depends more significantly on potassium than on sodium channel densities. However, the numerical simulations presented in the Appendix A agree with a common belief that in the large noise regime the contrary is true, i.e. sodium noise has a larger effect on the average firing rate compared to the potassium noise. This is consistent with the results derived in Chow and White (1996) in terms of the exit time problem. It is particularly intriguing that while the sodium channel stochasticity significantly affects the simple statistics of the average firing rate, particularly in the large noise regime (with channel numbers $N<1000$), the potassium variability keeps it mostly unaffected (with observable effects only in the small noise regime $N>1000$) but controls the overall distribution of the inter-spike intervals (that stays mostly unaffected by sodium variability). Thus the two ionic mechanisms contribute to the neuronal behavior in very different regimes corresponding to different neuronal sizes.

The behavior of the SQ model is influenced by the choice of transition probabilities p_{SQ} and p_{QS} depending on the source and magnitude of noise. Fig. 5 shows these probabilities as functions of applied current in the numerical simulation using LS method. Two observations can be made. First, as the applied current increases, probability p_{SQ} rapidly decreases to zero meaning that Q states will be rare for high currents. At the same time the probability p_{QS} rapidly increases to one implying that Q state will be quickly abandoned. This monotone behavior together with the relationship for $\mathbb{E}[ISI]=\mu_1+\mu_2 p_{SQ}/p_{QS}$ yields a monotone behavior of the average firing rate $1/\mathbb{E}[ISI]$ with respect to the applied current. Also, the curves for various sodium channel numbers (left on Fig. 5) show considerably less variation when compared to potassium channel numbers. Since we are in the regime of low variability this supports the observation that for large channel densities (small variability) potassium channel variability plays dominant role. However, for strong noise this situation is reversed and sodium variability plays more important role. We should note, however, that fluctuations that large may not be present in real neurons.

Parametric regime of small noise can also be studied using a linearization around the fixed point since small noise in the proximity of the steady state acts as a small perturbation of the state. Comparison of the effects of such perturbations in directions corresponding to sodium, potassium or applied current variability presented in the Appendix C confirms the relative importance of the potassium variability compared to sodium variability in low-noise regime.

3.4. Loss of memory

The numerical results shown in Fig. 5 (left panel) for the inferred SQ model transition rates suggest that a constraint $p_{SQ}+p_{QS}=1$ is valid in the regime of the small potassium noise with

$$p_{SQ}\approx e^{-I/\tau},\quad \tau\approx 4.5. \tag{11}$$

While the form of the transition probability agrees with a result of Ditlevsen and Greenwood (2012) where the firing probability in the Morris-Lecar model was assumed to have a sigmoidal shape (exponential in our case captures the tail of the sigmoid) the fact that transition probabilities add up to one is even more intriguing since it implies

$$p_{SQ}+p_{QS}=1 \Rightarrow p_{QS}=p_{SS} \quad \text{and} \quad p_{QQ}=p_{SQ}.$$

The above conditions impose a strong constraint on the Markovian process that in general depends on its current state but not on its history. Amazingly, this constraint means the future state of the system does not depend on its present state, i.e., there is no temporal correlation in the spike train (probability of an S state is the same no matter what state you came from). In such case the spike train can be represented by simple repeated flip of a biased coin with no memory rather than by a more complicated Markov model.

3.5. Quantitative inference of channel densities

Electrical recordings of real neurons driven by channel noise with deterministic inputs could be studied in connection with the simulation results in the Appendix A to relate the sodium and potassium channel densities. Given the input current and a time series of electrical activity of a neuron one may compute the average firing rate and use the surface relationship that gives the average firing rate dependence on the channel densities to assess the relationship between the channel variability of sodium channels and potassium channels, as depicted in Fig. 6.

A similar relationship holds also in the SQ model where the given average firing rate and constants μ_1 and μ_2 yield a relationship between transition probabilities p_{SQ} and p_{QS} in a form: $p_{SQ}=p_{QS}(\mathbb{E}[ISI]-\mu_1)/\mu_2$ that could be used to extract the correct

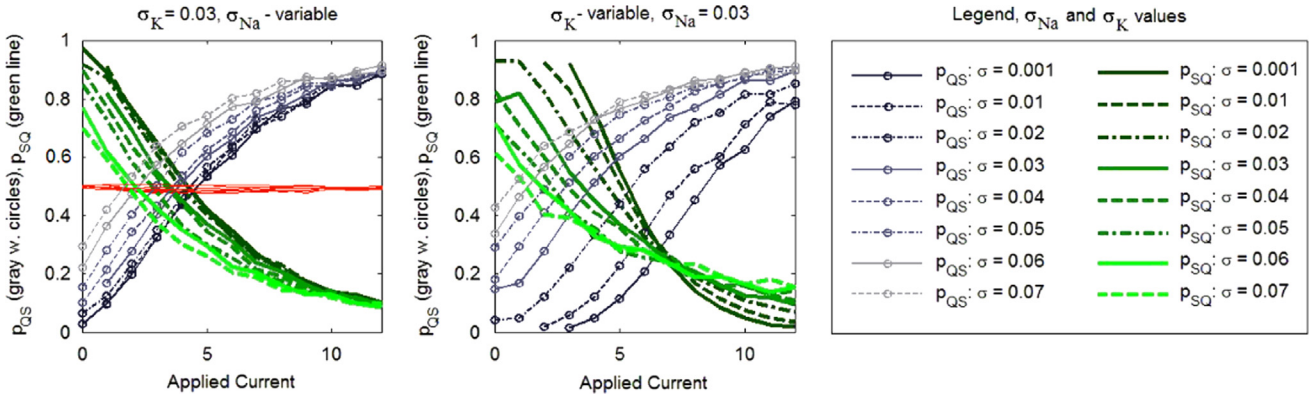

Fig. 5. Dependence of the transition probabilities on the applied current (LS simulation). Green curves correspond to p_{SQ} and gray curves with circles to p_{QS}. The panel on the left shows effects of changing the sodium variability with $\sigma_K=0.03$ ($N_K=1111$) and $\sigma_{Na}\in[0.001, 0.07]$. The panel on the right shows effects of changing potassium variability with $\sigma_{Na}=0.03$ ($N_{Na}=1111$) and $\sigma_K\in[0.001, 0.07]$. Red curves represent the arithmetic mean of p_{SQ} and p_{QS}. (For interpretation of the references to color in this figure caption, the reader is referred to the web version of this article.)

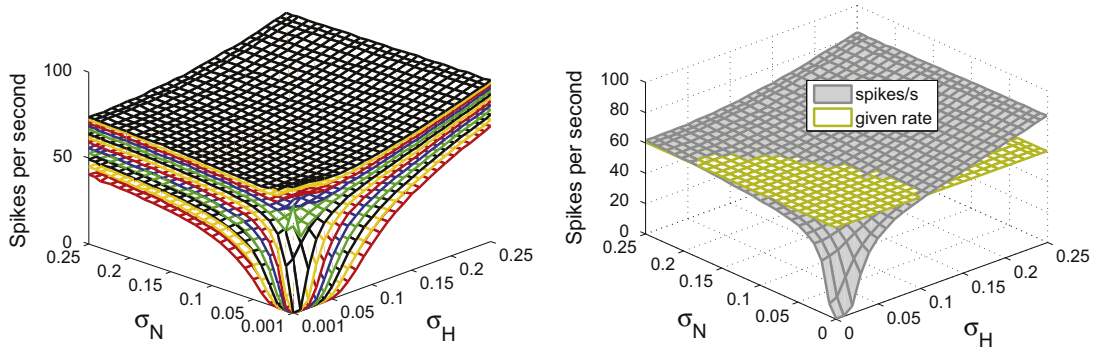

Fig. 6. The firing rate is a two dimensional function (surface) of sodium and potassium variability for any fixed value of applied current. This surface is plotted for $I = 0, 1, \ldots, 12\ \mu A/cm^2$ for the Fox method. The increase of the applied current results in the increase of the mean firing rate for all considered parameter values. The mean firing rate profile for $I = 6\ \mu A/cm^2$ intersected with a level-plane corresponding to the mean firing rate of 60 spikes/s.

branch on Fig. 5, determining the channel density. In a particular case when the constraint $p_{SQ} + p_{QS} = 1$ is valid, as observed in Fig. 5, we obtain

$$p_{SQ} = \frac{\mathbb{E}[ISI] - \mu_1}{\mu_2 + (\mathbb{E}[ISI] - \mu_1)}, \quad p_{QS} = \frac{\mu_2}{\mu_2 + (\mathbb{E}[ISI] - \mu_1)} \tag{11}$$

that could be linked back to a relationship between channel densities.

Two numbers are required to fit our model, the decay of the ISI and burst size distribution to imply the parameters of the SQ model. Note that once we understand the probabilistic laws behind the behavior of the neuron by means of the SQ model, corresponding to the parameters μ_1, μ_2, σ_1, σ_2, p_{SQ}, p_{QS}, we can characterize the average firing rate but at the same time this information also unravels much more about the behavior of the particular neuron, i.e., we may then estimate the likelihood of occurrence of particular burst pattern (for instance frequency of doublets) or compute probability that at a given impulse strength the neuron stays silent for a given period of time.

4. Conclusions

Many neurons, particularly those that are noisy, are thought to encode information by the average rate at which action potentials are fired. The average firing rate depends on the stochasticity of the channel dynamics, which is determined by the number of sodium and potassium channels and on the input stochasticity. However, a more accurate characterization of the electrical behavior of neurons requires more complex statistics that include distributions of interspike intervals or burst lengths. Our numerical simulations of channel noise as well as experimental results of input variability show that the interspike interval distribution may have a full range of shapes between multimodal and single-peaked depending on the noise regime.

Large neurons exhibit small sensitivity to individual channel dynamics and therefore are driven mostly by stochasticity in applied current as opposed to channel noise. However, applied noise in large neurons results in similar statistical patterns as channel noise in small neurons, i.e. induction or deletion of spikes and effects on ISI distribution shape (from multimodal to single-peaked according to noise magnitude) as analyzed in Paydarfar et al. (2006). We use the experimental recordings with large neurons under the input noise and study the structural similarities with our numerical simulations affected by channel noise. We explain this universality by a probabilistic model where the structural properties of noise enter via the parameter values. This model captures many characteristics of type II neuronal behavior under the influence of (Na or K) channel noise or input noise and is amenable to mathematical analysis.

The probabilistic model helps unravel how the regulation of neuronal activity in the presence of noise works and what are the key components of the process. In particular, there are three possible ways to regulate the average firing rate in type II neurons. First, one can regulate the period of firing when in the repetitively firing state by changing parameters of the system, e.g., the input current. Second, one can increase or decrease the probability of a transition from a quiescent state to a repetitively firing state. Finally, one can do the reverse: increase or decrease the probability of a transition from the repetitively firing state to a quiescent state. However, the latter two mechanisms are not independent and particularly for small potassium variability the transition probabilities are slaved by a constraint leading to a loss of temporal correlation in the spike train. This is demonstrated in our detailed numerical simulation results used to extract the dependencies of the transition rate probabilities between the spiking and quiescent state in the probabilistic model. An analogous experiment could be designed where a constant current is injected and transition probabilities are estimated from voltage traces. Repeating the experiment for different values of injected current but also for different neurons should reveal whether the relationship between transition rates is valid and how does the dependence on injected current compare with curves on Fig. 5.

Moreover, the mathematical model explains structural properties of the two highlighted experimentally obtained distributions (interspike interval and burst length distribution). The first property is that both the ISI distribution and the burst size distribution have exponential tails where the rate of decay is in an explicit relationship to the parameters of the probabilistic model. The second property is that the exponential decay is valid universally for the whole distribution (all modes) except for the height of the first mode of the ISI distribution that exceeds this prediction. Such a behavior has been observed in a study of sporadic apnea (Paydarfar and Buerkel, 1997).

Our numerical simulations confirm that sodium noise affects the average firing rate more than potassium noise for small neurons in accordance with the previous work that has explored the role of sodium channel variability (Chow and White, 1996; White et al., 2000; Mino et al., 2002). It is interesting to note, however, that potassium noise has comparable and even more significant effect on the mean firing rate for large neurons. Moreover, potassium stochasticity affects the ISI distribution more significantly than sodium stochasticity. When the potassium noise is small the ISI distribution is multimodal whereas as the amplitude of the potassium noise is increased, it causes the ISI histogram to become smoother and thus single-peaked matching previous findings for the input current variability (Paydarfar et al., 2006). This affects the regularity of spike timing as the multimodal distribution yields more predictable spike times compared to

single-peaked ISI distribution with the same variance. Therefore both Na and K channel densities significantly contribute to relevant statistical properties of the temporal neuronal behavior depending on their size. This is an experimental prediction that could be tested if one could accurately modify the number of channels within a neuron. On the other hand, the importance of applied noise can be tested using patch clamp experiments of neurons exposed to noisy stimuli. Knowledge of the channel response to applied current noise might be useful for developing and testing ionic models of neurons.

The Hodgkin–Huxley model is an example of a type II neuron, where the stable oscillations are born via a subcritical Hopf bifurcation yielding finite nonzero frequency of oscillations that is only weakly dependent on the size of the injected current. Thus, while it is reasonable to expect that our results will be applicable to other type II neurons, they may not be applicable to neurons (e.g. type I or III neurons) that show different dynamical behaviors. On the other hand, raising the variability of the input noise affects the sharpness of the transition to oscillations and thus makes type II neurons behave more like type I neurons. Neuronal models with a type I behavior, associated with a saddle-node bifurcation, have been studied in the presence of noise in Gutkin and Ermentrout (1998) for the θ-neuron with a multiplicative noise and in Lindner et al. (2003) for a normal form of the SN bifurcation perturbed by an additive Gaussian white noise focusing on the mean firing rate and the coefficient of variation of the ISI. Our preliminary work suggests that behavior similar to our observations could be seen for noisy type III neurons that show no periodic firing in the absence of noise, i.e., we observe excitation of the neuron due to noise, irregular firing of action potentials with frequency dependent on noise magnitude. Future work should focus on characterizing the behavior of type III neurons but also extending the study to neuronal networks of HH-type neurons where the sodium and potassium variability affect the properties of the network in relation to its topology as shown for instance in Ozer et al. (2009), Sun et al. (2011).

While our results suggest a general characterization of noisy firing in type II neurons, further work is needed to test our predictions both for the squid giant axon and for other neurons as well. Particularly, it has been argued that neurons in several different systems (e.g. the suprachiasmatic nucleus (Sim and Forger, 2007; Kononenko and Dudek, 2004), neocortical neurons (Llinas et al., 1991) and sensory receptors (Braun et al., 1994)) display behaviors that are similar to the behaviors we observe and it would be interesting to test our predictions further in these neuronal preparations.

It is important to test these principles in other models. Particularly the Morris-Lecar model has been subject to wide theoretical study, and for certain parameter ranges, it shows type II behavior. Rowat and Greenwood (2011) provides a detailed computational study of this model yielding some results that are compatible to our work. It would be interesting to characterize noisy firing in type I neurons, which have a different bifurcation structure than is found in our model. Some neurons show unconventional electrical activities (Belle et al., 2009) and it would be interesting to understand the role of noise in these systems as well.

Moreover, since the probabilistic model is efficient to simulate it is important to know how such a simple model could be coupled to represent a network of neurons. Pursuing this direction may be very useful for large-scale neuronal network simulations where the limits of modern technologies are reached.

Acknowledgments

The authors would like to thank John Clay for helpful discussions. This work is supported by AFOSR grant FA 9550-11-1-0165, program grant RPG 24/2012 from the Human Frontiers of Science (DBF) and travel support from the European Commission Marie Curie International Reintegration Grant PIRG04-GA-2008-239429 (KB). DP was supported by NIH R01 GM104987 and the Wyss Institute of Biologically Inspired Engineering. The funders had no role in study design, data collection and analysis, decision to publish, or preparation of the manuscript.

Appendix A. Computational methods for channel noise

The Hodgkin–Huxley model (Hodgkin and Huxley, 1952) describes the voltage of a neuron with the following equation:

$$C_m\frac{dV}{dt} = -g_{\mathrm{Na}}m^3h(V-V_{\mathrm{Na}}) - g_{\mathrm{K}}n^4(V-V_{\mathrm{K}}) - g_{\mathrm{L}}(V-V_{\mathrm{L}}) + I \qquad (A.1)$$

where V is the membrane potential, V_{Na}, V_{K} and V_{L} are the reversal potentials of sodium, potassium and leakage currents, g_{Na}, g_{K} and g_{L} are the corresponding maximum ion conductances, C_m is the membrane capacitance and I is the applied current, see Table A1.

The nonlinearities in the electric potential equation are believed to reflect a physical structure of sodium and potassium channels, i.e. that each channel consists of four gates (m, n and h type). The variables $x = m, n, h$ therefore capture probabilities that the corresponding gate is open and obey differential equations

$$\frac{dx}{dt} = \alpha_x(V)(1-x) - \beta_x(V)x \qquad (A.2)$$

where the growth rates for x and the parameter values (equilibrium reversal potentials, ion conductances, membrane capacitance), used throughout the work are taken from the original work of Hodgkin and Huxley (1952), see Table A1. The Hodgkin–Huxley model shows limit cycle oscillations, also called action potentials (AP) that exist for superthreshold applied currents. These oscillations are born via a subcritical Hopf bifurcation that is accompanied by the loss of stability of the quiescent state. For a range of medium-sized applied currents the system shows bistable behavior where both the steady state and the oscillations are stable. Action potential initiation is driven by activation of sodium channels and prevented by activation of potassium channels. For a stability analysis and a complete two-parameter bifurcation analysis of the Hodgkin–Huxley model see Guckenheimer and Labouriau (1993) and Hassard (1978).

While the numerical implementation of the deterministic Hodgkin–Huxley model is straightforward, there are multiple substantially different ways of simulating the model with noise. Each of the methods has some advantages and some limitations. The comparison of different KMC and LS methods can be found in the work of Bruce (2007).

Our simulations use the Hodgkin–Huxley model with its original parameters (Hodgkin and Huxley, 1952), displayed in Table A1. Each of the two methods (KMC and LS) considers both sodium channels (with two types of gates) and potassium channels (with a single type of gate). When using the KMC approach, the opening and closing of specific ion channel gate is simulated. We report N_{K} which is the total number of potassium channels used in our model (where $N = 4N_{\mathrm{K}}$ is the total number of potassium gates). We also report $N_{\mathrm{Na}} = H$, which is the total number of sodium channels as well as the number of sodium

Table A1
Parameters of the Hodgkin–Huxley model.

Constant	V_{Na}	V_{K}	V_{L}	g_{Na}	g_{K}	g_{L}	C_m
Value	115	−12	−10.613	120	36	0.3	1
Units	mV	mV	mV	mS cm^{-2}	mS cm^{-2}	mS cm^{-2}	μF cm^{-2}

inactivating gates. The total number of activating sodium gates is $M=3H$. When using the LS approach, individual ion channels are represented by the probability that a gate is in the open state. The amplitude of the random fluctuations in this probability is denoted by $\sigma_K = N_K^{-1/2}$ for potassium gates and $\sigma_{Na} = N_{Na}^{-1/2}$ for the sodium inactivating and activating gates. Thus increasing σ_K or σ_{Na} in the LS approach increases the amplitude of the noise, whereas increasing N or H increases the number of channels, which decreases the effects of stochasticity induced by single channel opening and closing on the models behavior. Thus, by varying N_{Na} and N_K in the KMC approach or by varying σ_K and σ_{Na} in the LS approach, we can control the strength of fluctuations in our simulations of the Hodgkin–Huxley model.

A.1. The kinetic Monte Carlo method

A traditional approach to study channel noise in a neuron is to use a kinetic Monte Carlo method, that tracks the opening and closing of individual channels (Clay and DeFelice, 1983; Chow and White, 1996; Schneidman et al., 1998; White et al., 2000; Skaugen and Walløe, 1979; Rowat, 2007). This method is particularly useful if the channel densities are low. However, for large channel densities the method becomes computationally expensive. In the KMC method, the opening and closing of individual ion channels is represented by memoryless chemical reactions occurring with transition rates α and β that depend on the electric potential. The channel densities, determined by the total number of gates ($M=3N_{Na}$, $N=4N_K$ and $H=N_{Na}$) are fixed, and determine the systems natural level of variability. We keep track of the total number of open gates of each type over time (Gillespie, 1977). This information assumes no gate correlations that may in some cases prove to be of importance as shown in Güler (2011).

Our implementation of the KMC method uses a so-called independent subunit approach (Goldwyn and Shea-Brown, 2011). Out of the total $M=3N_{Na}$ sodium activation gates we denote by m_1 the number of m-gates in each independent subunit with N_{Na} gates that are open at a given time. Since there are three independent subunits in sodium activation gates a total of $3m_1$ will be open at a given time. Similar notation h and n_1 is used for a number of inactivation sodium gates and potassium gates per subunit that are open at a given time. Note a change of meaning of m, n, and h from the original HH model. At each point in time where a transition to a new state occurs there are exactly six possible outcomes (an m-, n-, or h-gate opens or closes). All transition probabilities sum up to one at each transition point. The electric potential equation is modified to

$$C_m\frac{dV}{dt} = -g_{Na}\left(\frac{m_1}{N_{Na}}\right)^3\left(\frac{h}{N_{Na}}\right)(V-V_{Na}) - g_K\left(\frac{n_1}{N_K}\right)^4(V-V_K) - g_L(V-V_L)+I \quad (A.3)$$

where the probabilities that gates are open are substituted by a relative number of open gates of each type, i.e. m_1/N_{Na} , n_1/N_K , h/N_{Na}. The time interval Δt until the next transition is a random exponentially distributed number with $\Delta t \sim \mathrm{Exp}(\lambda)$ where λ is the sum of all transition rates as specified in the algorithm below.

KMC ALGORITHM:

1. Initialization: Specify initial values of V, number of open gates m_1, n_1, h and number of closed gates $N_{Na}-m_1$, N_K-n_1, $N_{Na}-h$.
2. Transition rates: Calculate the effective total rate of transition
$$\lambda = [\alpha_m(V)(N_{Na}-m_1)+\beta_m(V)m_1]+[\alpha_n(V)(N_K-n_1)+\beta_n(V)n_1] + [\alpha_h(V)(N_{Na}-h)+\beta_h(V)h] \quad (A.4)$$
and individual transition probabilities $p_m^+ = \alpha_m(V)(N_{Na}-m_1)/\lambda$ (the rate at which m-gate opens), $p_m^- = \beta_m(V)m_1/\lambda$ (the rate at which m-gate closes) and similarly for n_1 and h.
3. Time step: Generate two random numbers r_1, r_2 from a uniform distribution on interval [0,1]. The time to the next transition is: $\Delta t = -(1/\lambda)\log(r_1)$.
4. Integration: Integrate the electric potential equation between time t and $t+\Delta t$ using the Euler method.
5. Transition: Randomly choose one of six possible reactions with appropriate probabilities based on r_2 (Chow and White, 1996; Gillespie, 1977) where the reaction rates are
$$m_1 - 1 \overset{\beta_m(V)\cdot m_1}{\leftarrow} m_1 \overset{\alpha_m(V)\cdot(N_{Na}-m_1)}{\rightarrow} m_1+1 \quad (A.5)$$
$$n_1 - 1 \overset{\beta_n(V)\cdot n_1}{\leftarrow} n_1 \overset{\alpha_n(V)\cdot(N_K-n_1)}{\rightarrow} n_1+1 \quad (A.6)$$
$$h - 1 \overset{\beta_h(V)\cdot h}{\leftarrow} h \overset{\alpha_h(V)\cdot(N_{Na}-h)}{\rightarrow} h+1 \quad (A.7)$$
6. Loop: Repeat steps 2.-5. until the time reaches the terminal time (Table A2).

The level of variability in the KMC approach is captured by the individual channel numbers. If, say, $N_{Na} \gg 1$ then the single opening of gate h produces a change in the relative number of open gates of size $|(h\pm1)/N_{Na} - h/N_{Na}| = 1/N_{Na}$. Larger N_{Na} leads to a smaller change in the above expression, i.e., smaller variability. The simulation parameters including channel numbers can be found in Table A3.

A.2. The Langevin stochastic model

Computational methods based on the Langevin stochastic (LS) approach assume that the channel densities are sufficiently large so that a master equation is accurately approximated by a continuous model. The actual form of noise varies in the literature from multiplicative noise (Goldwyn and Shea-Brown, 2011; Fox, 1997; Ozer and Ekmekci, 2005; Schmid et al., 2006; Bazsó et al., 2003) to constant-amplitude noise (Bazsó et al., 2003; Saarinen et al., 2006), the proper form may be sometimes derived directly from the KMC approach (Linaro et al., 2011). Various mathematical studies regard a slow-fast system in the presence of noise as for instance (Hitczenko and Medvedev, 2009). To study channel noise

Table A2
The rates in the Hodgkin–Huxley model driving the channel dynamics of variables m, n, h.

Gate	m	n	h
$\alpha(V)$	$\frac{0.1(25-V)}{\exp\frac{25-V}{10}-1}$	$\frac{0.01(10-V)}{\exp(\frac{10-V}{10})-1}$	$0.07\exp\left(\frac{-V}{20}\right)$
$\beta(V)$	$4\exp\left(-\frac{V}{18}\right)$	$0.125\exp\left(-\frac{V}{80}\right)$	$\frac{1}{\exp\left(\frac{30-V}{10}\right)+1}$

Table A3
Numerical simulation parameters used in the LS and KMC methods.

	(1) LS	(2) KMC and LS
Input current I	$0, 0.5, 1, \ldots, 12$	$0, 0.5, 1, \ldots, 12$
Na variability	$\sigma_{Na} \in \{0, 0.001, 0.01, 0.02, \ldots, 0.25\}$	
	$N_{Na} \in [16, 10^6]$	$N_{Na} \in \{200, 400, \ldots, 4000\}$
K variability	$\sigma_K \in \{0, 0.001, 0.01, 0.02, \ldots, 0.25\}$	
	$N_K \in [16, 10^6]$)	$N_K \in \{200, 400, \ldots, 4000\}$
Simulation time	200 s	200 s

we input a multiplicative Gaussian random noise directly into the channel equations and not to the electric current equation as described in Fox and Lu (1994).

$$\frac{dx}{dt} = \alpha_x(V)(1-x) - \beta_x(V)x + g_x(t)\xi_x(t), \tag{A.8}$$

$$g_x^2(t) = 2\sigma^2 \frac{\alpha_x(V)\beta_x(V)}{\alpha_x(V)+\beta_x(V)}, \tag{A.9}$$

where σ^2 is σ_{Na}^2 or σ_K^2 for appropriate channel and $\xi_x(t)$, $x = m, n, h$ represents independent Gaussian white noise. Note that even though there are three gate variables, there are only two noise magnitudes. The independent parameters of LS model are therefore channel densities measured by N_{Na} and N_K and the constant applied current level I, see Table A3. The LS model is simple to implement numerically with an Euler method (or higher order methods), and the runtime only depends on a time step and not on the channel variability. If a random noise $\xi_x(t)$ results in a value of x outside [0,1] it is ignored and replaced by another randomly generated number and the integration step is repeated.

A.3. Numerical results for the channel noise

To understand the effects of channel noise, we performed large-scale simulations of both the LS and the KMC model with different channel densities and recorded the average firing rate and the exact spike times. We chose two sets of channel numbers, first one consisted of $N_K, N_{Na} \in [200, 4000]$ that was used to compare the firing rates for the LS and KMC method (see Table A3 for the parameter specification) and second consisted of a large range where N_K, N_{Na} varied from 16 to 10^6 to yield noise magnitudes $\sigma_K, \sigma_{Na} < 0.25$ (with equally distanced σ). The parameter range should cover the realistic channel densities that have been estimated for instance in Rogart (1981) for sodium channels. Note that the LS method is a faster method for large channel densities since the complexity of the algorithm stays independent of the channel densities unlike in the case of the KMC simulation.

Sample trajectories of our simulations are shown in Fig. C1 (A) for the LS approach (left) and the KMC approach (right) while keeping the noise parameters identical for the two approaches. To study the effects of noise, we also vary the current applied to the neuron (top to bottom). Without any applied current, the model without noise would show no action potentials. However, because of the stochastic channel dynamics in our model, rare spikes can be seen. As the current is increased the frequency of spikes increases, in contrast with the model without noise, where spikes would only be seen above input current $I \approx 6\,\mu A/cm^2$. These results are very similar to a wide range of other simulational and experimental studies that explore the role of noise in neurons (e.g. Clay and DeFelice, 1983; Chow and White, 1996; White et al., 2000; Schmid and Hanggi, 2007). We note that the KMC and LS methods yield similar, yet not identical results, with the most apparent difference for a large applied current. This indicates that, over the relevant timescales for neuronal firing, a sufficient number of channel openings and closings occur to allow the LS method to give a reasonably good approximation to the neuronal firing. Our simulations typically considered 16 to 10^6 channels, to ensure that the model generated action potentials. At lower densities, discrepancies could be found, as well as changes to the action potential shape.

The properties of stochastic neurons can be studied using various statistical moments or probability distributions based on the random electrical output of the neuron. Typically, the average firing rate over the simulation time is measured as well as a more detailed inter-spike interval distribution. A few statistical measures including average firing rate and ISI histogram were evaluated with results on average firing rate shown on Fig. A1 to help understand how channel noise affects the Hodgkin–Huxley neuron.

The deterministic model originally simulated by Hodgkin and Huxley corresponds to N_{Na} and N_K being infinite (the corresponding point in Fig. A1(C–D) would be infinitely far to the right and up) or σ_{Na} and σ_K being zero (that can be seen in Fig. A1(B) in the leftmost low corner). In the deterministic model, the firing rate is zero below a threshold value and then jumps to a nonzero firing frequency. This behavior can be observed in panels (B) as we approach the deterministic limit. Due to the much larger computational cost of the KMC method for large channel densities than the LS method, our KMC simulations capture a smaller region of noise levels. In parts (C–D) a comparison between the average firing rate obtained by the LS and the KMC method is explored, obtaining quantitatively similar results.

For low input currents, where the deterministic model would not show any action potentials, increasing stochasticity increases the firing rate. However, for high applied currents, this is not true

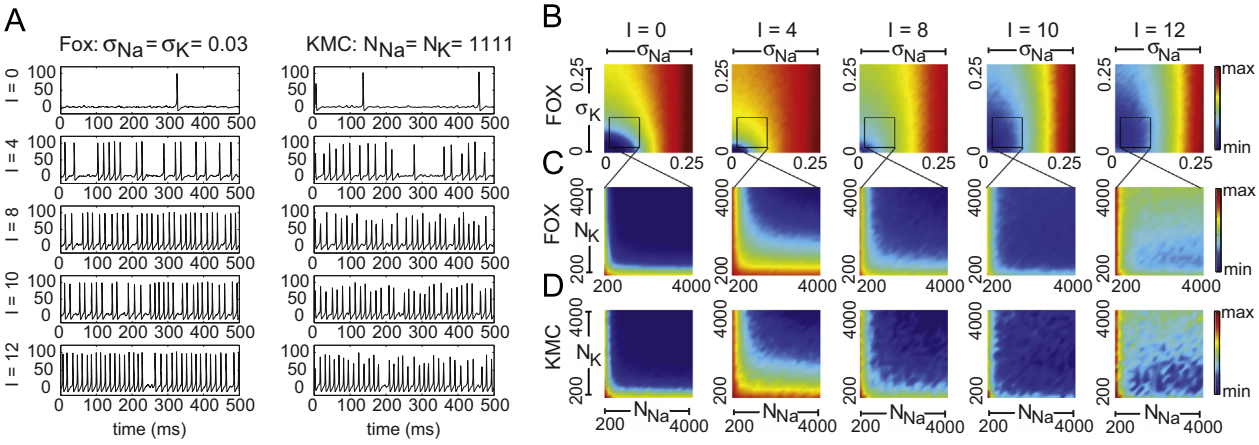

Fig. A1. Numerical results using the LS/Fox and KMC method. (A) Firing patterns in the stochastic Hodgkin–Huxley model. Voltage is plotted versus time (in ms). Both Langevin stochastic approach (LS/Fox) and the Kinetic Monte-Carlo (KMC) approach show spontaneous firing for subthreshold currents ($I = 0, 4\ \mu A/cm^2$) and suppression of oscillations for superthreshold currents ($I = 8, 10, 12\ \mu A/cm^2$). (B-D) Firing frequency dependence on the applied current and noise. Colorplots show mean firing rate as a function of noise magnitudes σ_{Na} on the horizontal axis and σ_K on the vertical axis (Fox method) where σ_K, σ_{Na} were chosen from [0.001, 0.25] that corresponds to N_K, N_{Na} from $[16, 10^6]$. Panels (C)–(D) show the firing rate for the LS and KMC method for a limited range of channel numbers N_{Na} and $N_K \in [200, 4000]$ marked as a black square on panels in (B). The colorscale for panels in (B) is set as min = {0, 0, 40, 60, 65} and max = {65, 80, 90, 90, 95} and for (C–D) as min = {0, 10, 50, 60, 65} and max = {45, 60, 70, 75, 75}.

in general anymore and a reversed stochastic resonance is observed (as in Paydarfar et al., 2006). In the low noise range variability (mainly in potassium channels) acts to stop action potentials therefore increasing variability decreases the average firing rate as visible on Fig. A1(C–D). On the other hand, in the strong noise range, firing is enhanced by variability because the average duration of the action potential is decreased due to large variability.

Changing the stochasticity of the sodium channels has stronger effects on the firing rate than potassium currents in the strong noise range. This can be easily seen in the panels of Fig. A1 (B) where the firing rate significantly changes as one proceeds horizontally in these graphs. On the other hand, for very small noise amplitudes, as the ones studied in Fig. A1(C–D), the opposite is true and the potassium noise affects the firing rate more than the sodium noise, see Fig. A1(C–D). This is supported by a mathematical argument in Appendix C for large neurons where we used linearization of the system to quantify the effects of different sources of noise to the neuronal dynamics. The results are intriguing as they imply that for different neurons with different channel densities different ionic mechanisms may be dominant.

Appendix B. Experimental methods for applied current noise

Large axons such as the squid giant axon show low levels of channel variability allowing them to generate regular temporal activity as a response to constant inputs. However, if the input current is random the axonal response becomes more noisy with characteristics similar to effects of channel noise in small neurons (Paydarfar et al., 2006).

The data from squid giant axons used in the present study are from previously published experiments (Paydarfar et al., 2006) and are publicly accessible at www.physionet.org. They were performed on squid giant axons from the North Atlantic squid (*Loligo pealei*) at the Marine Biological Laboratory in Woods Hole, MA using axial wire voltage- and current-clamp techniques with intracellular perfusion described in Clay and Shlesinger (1983). Stochastic input current had a form of summed independently generated excitatory and inhibitory polysynaptic currents with a given Poisson rate. Because an identical distribution was chosen for excitatory and inhibitory postsynaptic currents the mean current was equal to zero in every trial. However, the root mean square of the stimulus current I_{rms} was varied. Such input current excited a stochastic response of the axon that has been recorded and used for the construction of statistical distributions in the main text.

$$J=\begin{pmatrix} -g_{\mathrm{Na}}m^3h-g_{\mathrm{K}}n^4-g_{\mathrm{L}} & -3g_{\mathrm{Na}}m^2h(V-V_{\mathrm{Na}}) & -4g_{\mathrm{K}}n^3(V-V_{\mathrm{K}}) & -g_{\mathrm{Na}}m^3(V-V_{\mathrm{Na}}) \\ \alpha_m'(V)(1-m)-\beta_m'(V)m & -\alpha_m(V)-\beta_m(V) & 0 & 0 \\ \alpha_n'(V)(1-n)-\beta_n'(V)n & 0 & -\alpha_n(V)-\beta_n(V) & 0 \\ \alpha_h'(V)(1-h)-\beta_h'(V)h & 0 & 0 & -\alpha_h(V)-\beta_h(V) \end{pmatrix}.$$

The statistical distributions used in this work to characterize the electrical behavior of the North Atlantic squid axon in response to the variable inputs include distribution of inter-spike intervals and distribution of burst size, the latter capturing the number of spikes per burst in a spike train. We analyze data from experimental runs at $I_{\mathrm{rms}}=0.13, 0.2, 0.35, 0.43\ \mu\mathrm{A/cm}^2$ (already presented in Paydarfar et al., 2006) and compare their ISI distribution with a prediction of the SQ model. We find that the increase in input variability I_{rms} affects the interspike interval distribution shape that changes from a multimodal distribution to a single-peaked distribution as the input variability is increased. We also analyze yet unpublished recordings at $I_{\mathrm{rms}}=0.2\ \mu\mathrm{A/cm}^2$ to construct burst length distribution and ISI distribution in the main text and compare it with a theoretical prediction.

We also used previously published data of SCN neurons in rat hypothalamus (Kononenko and Dudek, 2004) to test the SQ model, even though the noise here may not come solely from neuronal inputs. These neurons show regular firing with large firing rate and irregular firing with low firing rate. The authors mention that "neurons with irregular activity may possess the same intrinsic mechanism of generation of spontaneous activity as regular-firing SCN neurons, but receive higher levels of inhibitory synaptic input". We propose one such mechanism (the SQ model) and study whether it gives a plausible explanation for the data.

Appendix C. Linear analysis of the HH model to quantify sensitivity to noise

The behavior of the Hodgkin–Huxley model with randomly perturbed variables V, m, n or h may be studied in a proximity of the steady state, where the trajectories may transition between the oscillatory and quiescent state. Due to the small size of the transition region and its proximity to the steady state we may study the linearized deterministic HH model and the influence of nonrandom perturbations in the V, m, n and h directions. These deterministic perturbations, will reveal to what extent is the system sensitive to small changes in one of the channel variables (m, n and h) or inputed current (I) that may in reality arise either from random or from nonrandom forces.

The linearization of the Hodgkin–Huxley system around the fixed point may be performed symbolically, however, the exact calculation is computed numerically because of the nonlinearities in the problem. The steady state is a solution of the system of algebraic equations parametrized by applied current I:

$$g_{\mathrm{Na}}m(V^*)^3h(V^*)(V^*-V_{\mathrm{Na}})+g_{\mathrm{K}}n(V^*)^4(V^*-V_{\mathrm{K}})+g_{\mathrm{L}}(V^*-V_{\mathrm{L}})=I, \tag{C.1}$$

$$m^*=\frac{\alpha_m(V^*)}{\alpha_m(V^*)+\beta_m(V^*)},\quad n^*=\frac{\alpha_n(V^*)}{\alpha_n(V^*)+\beta_n(V^*)},\quad h^*=\frac{\alpha_h(V^*)}{\alpha_h(V^*)+\beta_h(V^*)}, \tag{C.2}$$

where the first equation gives an identity for V^* and the steady states for gating variables are calculated from the remaining three equations. Linear stability of the fixed point $(V^*,m^*,n^*,h^*)=(V^*,m(V^*),n(V^*),h(V^*))$ is determined by the real parts of eigenvalues of the Jacobi matrix $J^*=J(V^*,m^*,n^*,h^*)$ at the steady state, where $J=J(V,m,n,h)$ has a form

For the studied range of applied currents [0,12] there are always two real negative eigenvalues $\lambda_1\ll\lambda_2<0$ with corresponding eigenvectors v_1, v_2. Two remaining eigenvalues $\lambda_3=\mu_1+i\mu_2$ and $\lambda_4=\mu_1-i\mu_2$ are complex with a real part changing sign from $\mu_1<0$ to $\mu_1>0$ at the point of subcritical Hopf bifurcation. The linear locally invariant subspace $\mathcal{O}$, demonstrated on Fig. C1(A) (the name reflects the oscillatory character of trajectories in $\mathcal{O}$) is a 2-dimensional eigenspace spanned by the real and imaginary parts of eigenvectors v_3 and v_4, i.e., $w_3=\mathrm{Re}(v_3)$, $w_4=\mathrm{Im}(v_4)$.

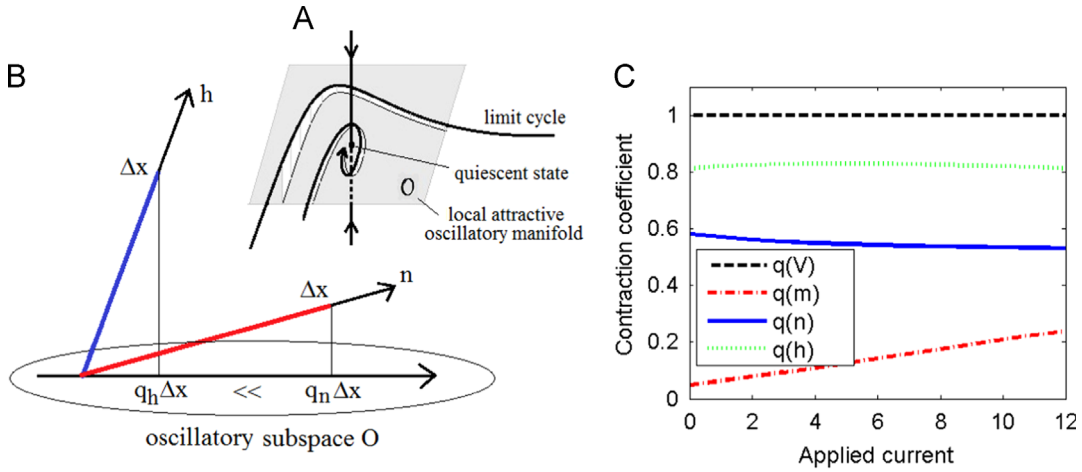

Fig. C1. Effects of small perturbations in directions V, m, n, h. (A) A demonstration in 3D. Gray plane corresponds to the oscillatory part of the system and is spanned by vectors u_3 and u_4. Due to the attractiveness of this plane, trajectories close to the plane will approach it. Linear stability determines whether the trajectory oscillates towards or away from the fixed point. (B) Schematic figure of two directions (n and h) with different sizes of coefficient q (for the sake of clarity we have not included the third vector m). (C) Values of coefficient of contraction q with a perturbation applied in four possible directions.

The linear subspace $\mathcal{O}$ has a property that trajectories starting close to the steady state approach this plane and the projection of trajectories on $\mathcal{O}$ oscillates (stability of oscillations depends on the sign of μ_1).

To find an orthonormal basis of $\mathcal{O}$ we use a Gramm–Schmidt orthonormalization process on $\{u_3, u_4\}$ and obtain:

$$u_3 = \frac{w_3}{\|w_3\|}, \quad u_4 = \frac{w_4 - (u_3, w_4)u_3}{\|w_4 - (u_3, w_4)u_3\|} \tag{C.3}$$

with approximate values

$$u_3 \approx (0.999976, 0.006497, -0.000377, 0.002275),$$
$$u_4 \approx (-0.001744, -0.049225, -0.581272, 0.812217), \quad \text{for } I = 0, \tag{C.4}$$

$$u_3 \approx (0.999937, 0.01076, 0.001774, -0.002003),$$
$$u_4 \approx (0.005183, -0.240226, -0.531525, 0.812247), \quad \text{for } I = 12. \tag{C.5}$$

The eigenvalues λ_i are

$$\lambda_1 \approx -4.68, \quad \lambda_3 \approx -0.20 + 0.38i \approx \overline{\lambda_4}, \quad \lambda_2 \approx -0.12, \quad \text{for } I = 0, \tag{C.6}$$

$$\lambda_1 \approx -4.87, \quad \lambda_3 \approx 0.04 + 0.60i \approx \overline{\lambda_4}, \quad \lambda_2 \approx -0.14, \quad \text{for } I = 12. \tag{C.7}$$

Given that variables V, m, n, h are represented by unit vectors e_1, e_2, e_3, e_4 in $\mathbb{R}^4$, where e_i has entry one in i-th coordinate and zeros otherwise then projections of these vectors onto the oscillatory manifold $\mathcal{O}$ can be written as

$$P_{\mathcal{O}}\{e_i\} = (u_3, e_i)u_3 + (u_4, e_i)u_4. \tag{C.8}$$

Therefore a projection $P_{\mathcal{O}}\{e_i\}$ of a normalized vector in the i-th direction (e_i) has length $q(e_i)$ where

$$q(e_i) = \sqrt{(u_3, e_i)^2 + (u_4, e_i)^2}. \tag{C.9}$$

Fig. C1(B) shows schematically a difference in effect of perturbation of length Δx in variables m and h in terms of $q(m)$ and $q(n)$. Fig. C1(C) shows the numerical calculation of quantities $q(x)$ where $x = V, m, n, h$ showing a large disproportion between the size of q (m) and the other projection lengths for subthreshold applied current ($q(m) \ll q(n) < q(h) < q(V)$) thus confirming that small noisy perturbations in Na direction have less impact than in K direction.

References

Bazsó, F., Zalányi, L., Csárdi, G., 2003. Channel noise in Hodgkin–Huxley model neurons. Phys. Lett. A 311 (1), 13–20. http://dx.doi.org/10.1016/S0375-9601(03)00454-7.

Belle, M.D.C., Diekman, C.O., Forger, D.B., Piggins, H.D., 2009. Daily electrical silencing in the mammalian circadian clock. Sci. Signal. 326 (5950), 281. http://dx.doi.org/10.1126/science.1169657.

Braun, H.A., Wissing, H., Schäfer, K., Hirsch, M.C., 1994. Oscillation and noise determine signal transduction in shark multimodal sensory cells. Nature 367 (6460), 270–273. http://dx.doi.org/10.1038/367270a0.

Bruce, I.C., 2007. Implementation issues in approximate methods for stochastic Hodgkin–Huxley models. Ann. Biomed. Eng. 35 (2), 315–318. http://dx.doi.org/10.1007/s10439-006-9174-9.

Chow, C.C., White, J.A., 1996. Spontaneous action potentials due to channel fluctuations. Biophys. J. 71 (6), 3013–3021. http://dx.doi.org/10.1016/S0006-3495(96)79494-8.

Clay, J.R., Shlesinger, M.F., 1983. Effects of external cesium and rubidium on outward potassium currents in squid axons. Biophys. J. 12, 43–53. http://dx.doi.org/10.1016/S0006-3495(83)84367-7.

Clay, J.R., DeFelice, L.J., 1983. Relationship between membrane excitability and single channel open-close kinetics. Biophys. J. 42 (2), 151–157. http://dx.doi.org/10.1016/S0006-3495(83)84381-1.

Ditlevsen, S., Greenwood, P., 2012. The Morris–Lecar neuron model embeds a leaky integrate-and-fire model. J. Math. Biol. 2, 239–259. http://dx.doi.org/10.1007/s00285-012-0552-7.

Faisal, A.A., Selen, L.P.J., Wolpert, D.M., 2008. Noise in the nervous system. Nat. Rev. Neurosci. 9 (4), 292–303. http://dx.doi.org/10.1038/nrn2258.

Fox, R.F., Lu, Y., 1994. Emergent collective behavior in large numbers of globally coupled independently stochastic ion channels. Phys. Rev. E 49 (4), 3421. http://dx.doi.org/10.1103/PhysRevE.49.3421.

Fox, R.F., 1997. Stochastic versions of the Hodgkin–Huxley equations. Biophys. J. 72 (5), 2068–2074. http://dx.doi.org/10.1016/S0006-3495(97)78850-7.

Gillespie, D.T., 1977. Exact stochastic simulation of coupled chemical reactions. J. Phys. Chem. US 81 (25), 2340–2361. http://dx.doi.org/10.1021/j100540a008.

Goldwyn, J.H., Shea-Brown, E., 2011. The what and where of adding channel noise to the Hodgkin–Huxley equations. PLoS Comput. Biol. 7 (11), e1002247. http://dx.doi.org/10.1371/journal.pcbi.1002247.

Gong, Y., Xie, Y., Hao, Y., 2009. Coherence resonance induced by non-Gaussian noise in a deterministic Hodgkin–Huxley neuron. Phys. A 388 (18), 3759–3764. http://dx.doi.org/10.1016/j.physa.2009.05.045.

Guckenheimer, J., Labouriau, I.S., 1993. Bifurcation of the Hodgkin and Huxley equations: a new twist. B. Math. Biol. 55 (5), 937–952. http://dx.doi.org/10.1007/BF02460693.

Güler, M., 2011. Persistent membranous cross correlations due to the multiplicity of gates in ion channels. J. Comput. Neurosci. 31 (3), 713–724. http://dx.doi.org/10.1007/s10827-011-0337-9.

Gutkin, B.S., Ermentrout, G.B., 1998. Dynamics of membrane excitability determine interspike interval variability: a link between spike generation mechanisms and cortical spike train statistics. Neural Comput. 10 (5), 1047–1065. http://dx.doi.org/10.1162/089976698300017331.

Hassard, B., 1978. Bifurcation of periodic solutions of the Hodgkin–Huxley model for the squid giant axon. J. Theor. Biol. 71 (3), 401–420. http://dx.doi.org/10.1016/0022-5193(78)90168-6.

Hitczenko, P., Medvedev, G.S., 2009. Bursting oscillations induced by small noise. SIAM J. Appl. Math. 69 (5), 1359–1392. http://dx.doi.org/10.1137/070711803.

Hodgkin, A.L., 1948. The local electric changes associated with repetitive action in a non-medullated axon. J. Physiol. 107 (2), 165–181.
Hodgkin, A.L., Huxley, A.F., 1952. A quantitative description of membrane current and its application to conduction and excitation in nerve. J Physiol. 117 (4), 500. http://dx.doi.org/10.1007/BF02459568.
Kononenko, N.I., Dudek, F.E., 2004. Mechanism of irregular firing of suprachiasmatic nucleus neurons in rat hypothalamic slices. J. Neurophys. 91 (1), 267–273.
Lee, S.-G., Kim, S., 1999. Parameter dependence of stochastic resonance in the stochastic Hodgkin–Huxley neuron. Phys. Rev. E. 60 (1), 826. http://dx.doi.org/10.1103/PhysRevE.60.826.
Lindner, B., Longtin, A., Bulsara, A., 2003. Analytic expressions for rate and cv of a type i neuron driven by white gaussian noise. Neural Comput. 15 (8), 1761–1788. http://dx.doi.org/10.1162/08997660360675035.
Linaro, D., Storace, M., Giugliano, M., 2011. Accurate and fast simulation of channel noise in conductance-based model neurons by diffusion approximation. PLoS Comput. Biol. 7 (3), e1001102. http://dx.doi.org/10.1371/journal.pcbi.1001102.
Llinas, R.R., Grace, A.A., Yarom, Y., 1991. In vitro neurons in mammalian cortical layer 4 exhibit intrinsic oscillatory activity in the 10-to 50-Hz frequency range. Proc. Natl. Acad. Sci. USA 88 (3), 897–901. http://dx.doi.org/10.1073/pnas.88.8.3510-c.
Longtin, A., Bulsara, A., Moss, F., 1991. Time-interval sequences in bistable systems and the noise-induced transmission of information by sensory neurons. Phys. Rev. Lett. 67 (5), 656–659. http://dx.doi.org/10.1103/PhysRevLett.67.656.
Mino, H., Rubinstein, J.T., White, J.A., 2002. Comparison of algorithms for the simulation of action potentials with stochastic sodium channels. Ann. Biomed. Eng. 30 (4), 578–587. http://dx.doi.org/10.1114/1.1475343.
Ozer, M., Ekmekci, N.H., 2005. Effect of channel noise on the time-course of recovery from inactivation of sodium channels. Phys. Lett. A 338 (2), 150–154. http://dx.doi.org/10.1016/j.physleta.2005.02.039.
Ozer, M., Perc, M., Uzuntarla, M., 2009. Controlling the spontaneous spiking regularity via channel blocking on Newman–Watts networks of Hodgkin–Huxley neurons. Europhys. Lett. 86 (4), 40008 ⟨http://dx.doi.org/10.1209/0295-5075/86/40008⟩.
Paydarfar, D, Forger, D.B., Clay, J.R., 2006. Noisy inputs and the induction of on-off switching behavior in a neuronal pacemaker. J. Neurophysiol. 96 (6), 3338–3348. http://dx.doi.org/10.1152/jn.00486.2006.
Paydarfar, D., Buerkel, D.M., 1997. Sporadic apnea: paradoxical transformation to eupnea by perturbations that inhibit inspiration. Med. Hypotheses 49 (1), 19–26. http://dx.doi.org/10.1016/S0306-9877(97)90246-2.
Pikovsky, A.S., Kurths, J., 1997. Coherence resonance in a noise-driven excitable system. Phys. Rev. Let. 78 (5), 775–778. http://dx.doi.org/10.1103/PhysRevLett.78.775.
Rogart, R., 1981. Sodium channels in nerve and muscle membrane. Annu. Rev. Physiol. 43 (1), 711–725. http://dx.doi.org/10.1146/annurev.ph.43.030181.003431.
Rowat, P., 2007. Interspike interval statistics in the stochastic Hodgkin–Huxley model: coexistence of gamma frequency bursts and highly irregular firing. Neural Comput. 19 (5), 1215–1250. http://dx.doi.org/10.1162/neco.2007.19.5.1215.
Rowat, P.F., Greenwood, P.E., 2011. Identification and continuity of the distributions of burst-length and interspike intervals in the stochastic Morris–Lecar neuron. Neural Comput. 23 (12), 3094–3124. http://dx.doi.org/10.1162/NECO_a_00209.
Saarinen, A., Linne, M.L., Yli-Harja, O., 2006. Modeling single neuron behavior using stochastic differential equations. Neurocomputing 69 (10), 1091–1096. http://dx.doi.org/10.1016/j.neucom.2005.12.052.
Schmid, G., Hanggi, P., 2007. Intrinsic coherence resonance in excitable membrane patches. Math. Biosci. 207 (2), 235–245. http://dx.doi.org/10.1016/j.mbs.2006.08.024.
Schmid, G., Goychuk, I., Hänggi, P., 2006. Capacitance fluctuations causing channel noise reduction in stochastic Hodgkin–Huxley systems. Phys. Biol. 3 (4), 248. http://dx.doi.org/10.1088/1478-3975/3/4/002.
Schneidman, E., Freedman, B., Segev, I., 1998. Ion channel stochasticity may be critical in determining the reliability and precision of spike timing. Neural Comput. 10 (7), 1679–1703. http://dx.doi.org/10.1162/089976698300017089.
Sim, C.K., Forger, D.B., 2007. Modeling the electrophysiology of suprachiasmatic nucleus neurons. J. Biol. Rhythm. 22 (5), 445–453.
Skaugen, E., Walløe, L., 1979. Firing behaviour in a stochastic nerve membrane model based upon the Hodgkin–Huxley equations. Acta Physiol. Scand. 107 (4), 343–363. http://dx.doi.org/10.1111/j.1748-1716.1979.tb06486.x.
Stiefel, K.M., Englitz, B., Sejnowski, T.J., 2012. Origin of intrinsic irregular firing in cortical interneurons. Proc. Natl. Acad. Sci. 110 (19), 7886–7891 ⟨http://dx.doi.org/10.1073/pnas.1305219110⟩.
Sun, X.J., Lei, J.Z., Perc, M., Lu, Q.S., Lv, S.J., 2011. Effects of channel noise on firing coherence of small-world Hodgkin–Huxley neuronal networks. Eur. Phys. J. B. 79, 61–66.
Tateno, T., Harsch, A., Robinson, H.P.C., 2004. Threshold firing frequency-current relationships of neurons in rat somatosensory cortex: type 1 and type 2 dynamics. J. Neurophysiol. 92 (4), 2283–2294. http://dx.doi.org/10.1152/jn.00109.2004.
Verveen, A.A., Derksen, H.E., 1968. Fluctuation phenomena in nerve membrane. Proc. IEEE 56 (6), 906–916. http://dx.doi.org/10.1109/PROC.1968.6443.
White, J.A., Rubinstein, J.T., Kay, A.R., 2000. Channel noise in neurons. Trends Neurosci. 23 (3), 131–137. http://dx.doi.org/10.1016/S0166-2236(99)01521-0.

Update

Journal of Theoretical Biology
Volume 373, Issue , 21 May 2015, Page 132

DOI: https://doi.org/10.1016/j.jtbi.2015.03.013

Journal of Theoretical Biology 373 (2015) 132

Contents lists available at ScienceDirect

Journal of Theoretical Biology

journal homepage: www.elsevier.com/locate/yjtbi

Erratum

Erratum to: Characterizing spiking in noisy type II neurons [J. Theor. Biol. 365 (2015) 40–54]

Katarína Bod'ová [a,*], David Paydarfar [b,c], Daniel B. Forger [d]

[a] Institute of Science and Technology Austria (IST Austria), Am Campus 1, Klosterneuburg A-3400, Austria
[b] Department of Neurology, University of Massachusetts Medical School, Worcester, MA, United States
[c] Wyss Institute for Biologically Inspired Engineering, Harvard University, Boston, MA, United States
[d] Department of Mathematics and Department for Computational Medicine and Bioinformatics, University of Michigan, Ann Arbor, MI, United States

Formula (4) on page 43 for the variance of the ISI distribution is missing an additional term. Because the distribution is a mixture of random variables X_k with probabilities p_k each corresponding to a realization of a particular number of Q states between the successive S states, the derivation should be as follows:

$$\begin{aligned}\mathrm{Var}[\mathrm{ISI}] &= \sum_{k=0}^{\infty} p_k \mathbf{E}[(X_k - \mathbf{E}[\mathrm{ISI}])^2] = \sum_{k=0}^{\infty} p_k \mathbf{E}[(X_k - \mathbf{E}[X_k] + \mathbf{E}[X_k] - \mathbf{E}[\mathrm{ISI}])^2] \\ &= \sum_{k=0}^{\infty} p_k \mathbf{E}[(X_k - \mathbf{E}[X_k])^2] + \sum_{k=0}^{\infty} p_k (\mathbf{E}[X_k] - \mathbf{E}[\mathrm{ISI}])^2 \\ &\quad + 2(\mathbf{E}[X_k] - \mathbf{E}[\mathrm{ISI}]) \sum_{k=0}^{\infty} p_k \mathbf{E}[(X_k - \mathbf{E}[X_k])] \\ &= \sum_{k=0}^{\infty} p_k \mathrm{Var}[X_k] + \sum_{k=0}^{\infty} p_k \left[(\mu_1 + k\mu_2) - \left(\mu_1 + \frac{p_{SQ}}{p_{QS}} \mu_2 \right) \right]^2\end{aligned}$$

where the cross term is equal to zero due cancellation of terms $\mathbf{E}[X_k]$ inside the sum. The following series

$$\sum_{k=1}^{\infty} x^k = \frac{x}{1-x}, \quad \sum_{k=1}^{\infty} k x^k = \frac{x}{(1-x)^2}, \quad \sum_{k=1}^{\infty} k^2 x^k = \frac{x(1+x)}{(1-x)^2}$$

lead to

$$\mathrm{Var}[\mathrm{ISI}] = \sigma_1^2 + \frac{p_{SQ}}{p_{QS}} \sigma_2^2 + \frac{p_{SQ}}{p_{QS}^2} \mu_2^2 (2 - p_{SQ} - p_{QS}) > \sigma_1^2 + \frac{p_{SQ}}{p_{QS}} \sigma_2^2.$$

Using the above formula the best fit for the ISI distribution of the SCN neuron (Fig. 3C and D) looks undistinguishable from the fit in the original paper, while the fitted coefficients for σ_2 in Table 1 (last column) change from values (57.77, 93.01, 55.07, 97.30) to (68.94, 93.46, 69.93, 94.04).

DOI of original article: http://dx.doi.org/10.1016/j.jtbi.2014.09.041
* Corresponding author.

http://dx.doi.org/10.1016/j.jtbi.2015.03.013
0022-5193/© 2015 The Authors. Published by Elsevier Ltd. All rights reserved.